COARSE-GRAINED KINETIC MODELING OF SEMI-CRYSTALLINE, NETWORK, AND NANOCOMPOSITE POLYMER SYSTEMS

A Dissertation

Presented to the Faculty of the Graduate School

of Cornell University

In Partial Fulfillment of the Requirements for the Degree of

Doctor of Philosophy

by

Brian James Pasquini

January 2009

COARSE-GRAINED KINETIC MODELING OF SEMI-CRYSTALLINE, NETWORK, AND NANOCOMPOSITE POLYMER SYSTEMS

Brian James Pasquini, Ph. D.

Cornell University 2009

A coarse-grained kinetic simulation approach is used to better understand dynamics of entangled polymers during tensile strain experiments of a diverse range of polymer systems. Building on two previous meso-scale simulation models from literature, the polymer systems studied include semi-crystalline, polymer network, and nanocomposite systems. One of these models (Smith and Termonia) formulates the free energy of an entanglement network based exclusively on interactions between neighboring entanglement points and uses temporary bonds which break as the simulation progresses to recover a semi-crystalline stress response. Another method (Terzis, Theodorou and Stroeks) treats the coarse-grained units as delocalized polymer density clouds and formulates an expression for the free energy based on local polymer density. Both methods have been studied and compared to a simple model system, revealing semi-crystalline and soft rubbery behaviors with and without the temporary bond, respectively. Additionally, elements of the existing entanglement network models have been extended in the two following ways: (1) The temporary bond from Smith and Termonia's model is combined with the DCM framework to simulate rigid domains within a matrix of soft polymer network. The modulus of the additional bond sets the elastic properties of the rigid domain, and entanglement

relaxation using the DCM assures local deformation remains consistent with the bulk polymer density. The effect of the size of rigid domain on initial modulus is reported. (2) Secondly, the role of entanglements in polymer networks is studied by employing different representations of entanglements, including non-affine tethering from theoretical models and the introduction of an entanglement bond potential acting internally at each entanglement. This potential mimics the non-affine tethering from network theories, and in combination with slippage shows qualitative agreement to Non-Affine Slip-Tube behavior. This polymer network framework can easily be extended to study various elements of polymer architecture, while incorporating realistic network behavior.

BIOGRAPHICAL SKETCH

Brian Pasquini began studying Chemical Engineering at Northwestern University. Graduating in 2003, he had worked on two undergraduate research projects: "Modeling of Cell Migration in the Presence of Drug Diffusion" with Prof. Lonnie Shea, and "3D Atom-Probe Study of Tungsten Disulfide Nanotubes" with Prof. David Seidman. He began work in the field of polymers as a graduate student at the Department of Chemical and Biomolecular Engineering at Cornell University, on the project contained in this thesis, "Coarse-Grained Kinetic Modeling of Semi-Crystalline, Network, and Nanocomposite Polymer Systems," under the advice of Professors Yong Joo and Fernando Escobedo.

Following the completion of his Ph. D. Brian plans to continue phenomenological modeling as a scientist at SciTec Inc. in Princeton NJ.

To Olivia and Tigerlilly.

ACKNOWLEDGMENTS

The author would like to acknowledge his advisors, Prof. Yong Lak Joo and Prof. Fernando A. Escobedo for their guidance, both technical and professional. In addition, for their selection of this thesis topic the author is particularly grateful. It has allowed him five years of challenging and rewarding work, which more notably has always been fun.

The author would like to thank each of the members of the Joo and Escobedo Research Groups, as colleagues and friends.

The author would like to acknowledge Prof. Claude Cohen, Prof. David T. Grubb and members of the Cohen Research Group for their significant contributions to this research.

Finally, the author would like to express his gratefulness of the U.S. Department of Education for funding through the Graduate Assistance In Areas Of National Need (*GAANN*) Fellowship Program.

TABLE OF CONTENTS

LIST OF FIGURES

LIST OF ABBREVIATIONS

Temporary Bond Model	TBM
Density Cloud Model	DCM
Self-Consistent Field [Theory]	SCF
Non-Affine Tube	NAT
Non-Affine Slip-Tube	NAST
Polyethylene	PE
Polypropylene	PP
Polyamide	PA
Poly(methyl methacrylate)	PMMA
Reverse Monte Carlo	RMC
Kinetic Monte Carlo	KMC
Monte Carlo	MC
Molecular Dynamics	MD
Molecular Weight	MW
Nanometer	nm
Gigapascal	GPa
Megapascal	MPa
Ultra High Molecular Weight	UHMW

LIST OF SYMBOLS

ΔA_{event}	Change in free energy associated with kinetic event
A_{total}	Total free energy of an entanglement network
A_0	Initial entanglement network cross-sectional area
dAes/dl	Derivative of free energy with respect to length
C	RMC artificial internal energy parameter
$C1$, $C2$	Parameters from modifying rate of kinetic events
F	Force of a polymer segment
k_B	Boltzmann constant
K	Temporary bond force constant
l	Statistical segment length
L^*	Inverse Langevin
L^*_{pade}	Padé approximate for the Inverse Langevin
m_p	Number of segments of tethering virtual chain
m_0	Number of segments of non-affine tethering at zero strain
m_α	Number of segments of non-affine tethering in dimension α
MW	Molecular weight
MW_e	Molecular weight between entanglements
$MW_{correct}$	Target molecular weight of RMC algorithm
n	Number of statistical segments
N_e	Number of statistical segments between entanglements
p	Number of segments between tethering points
$P(\boldsymbol{R},\boldsymbol{R}_{e1},\boldsymbol{R}_{e2},N_e)$	Probability of finding a conformation of an ideal chain with one sections of the chain $\boldsymbol{R}_{e1}$ and $\boldsymbol{R}_{e2}$ and overall chain conformation

	$\boldsymbol{R}$ and total number of segments N_e
$P(\boldsymbol{R};n)$	Probability of finding a chain with n segments stretched to $\boldsymbol{R}$
r	Polymer segment stretch distance; Rate of a kinetic event
$r_{correct}$	Target stretch distance of RMC algorithm
T	Temperature
U	Activation energy of kinetic event
$U_{randomcoil}$	Artificial internal energy of random coil RMC algorithm
$U_{molecularweight}$	Arificial internal energy for molecular weight RMC algorithm
α	A principle dimension in Cartesian coordinate space
ε	Strain
ε_y	*Y*-dimension component of strain
λ_α	Elongation in dimension α
ρ	Polymer bulk density
ρ_m	Polymer density parameter of simplified potential
ρ_0	Target polymer density of simplified potential
σ	Stress
σ_y	*Y*-dimension component of stress
υ	Thermal vibration frequency

PREFACE

While the overall objective of this thesis project -- to develop a coarse-grained kinetic model for entangled polymer systems – has remained constant, the specific systems being simulated have evolved with the discoveries along the way. Considering this, a chronological perspective of this work can be insightful.

Work on this thesis project began with two models from literature in mind, the Temporary Bond Model (TBM) of Smith and Termonia and the Density Cloud Model (DCM) of Terzis, Theodorou and Stroeks. Particularly in mind was the apparent ability of these models to simulate complex phenomena such as the impressive mechanical properties of spider silk, in the case of the TBM, and the failure of an adhesive interface, in the case of the DCM. However, to understand these models more closely meant a simplification in the systems treated, and a careful study of each individual element. The vehicle for this study became a detailed comparison of the two models (Chapter 2), something that seemed feasible considering the original formulations of each were used to model semi-crystalline polymers.

This led to the extension of the TBM to three dimensions and to studying the spatial discretization of the density cloud integration for the DCM, the latter proving to be the much more challenging objective. Achieving a consistent stress response over multiple stress cycles occupied the initial portion of research time. The challenge arose because the simulations were computationally expensive, and also because dominant numerical effects from finite size effects, spatial discretization, and overpowering density cloud equation of state could not be distinguished

independently. When the desired effects were believed to have been achieved, the result was a soft rubbery response for the DCM, one that seemed to capture realistic non-affine slip-tube behavior of polymer networks. The inherent non-affine behavior of the density clouds was shortly dispelled, but a major twist in the polymer system of interest resulted. Recovering a realistic polymer network response from and entanglement network simulation became a major goal.

Alongside simulation of polymer networks, another complexity was added in attempts to highlight the advantages of the DCM. This complexity was rigid domains using clusters of temporary bond elements from the TBM. This system is the spiritual combination of the two models studied.

Rather than a quantitative study of an increasingly complex system, this work builds on previous efforts through focusing more closely on the existing elements. By doing so, this effort demonstrates a set of tools for incorporating molecular details into the simulation of polymer systems as diverse as semi-crystalline, network and nanocomposites.

CHAPTER 1
INTRODUCTION

1.1 Objective

The objective of the following study is to develop a coarse-grained model towards the simulation of structurally complex polymer systems. It is desired to accomplish this through the use of fundamental polymer properties, derived from the molecular details of the system, to maintain a strong connection between microscopic representation and macroscopic properties.

This chapter contains an overview of fundamental concepts relevant to polymer simulation, followed by a review of the Temporary Bond Model (TBM) and Density Cloud Model (DCM) from literature. Also contained is a review of polymer network theories, and a mention of other molecular based simulation methods motivated by connecting molecular details to macroscopic phenomena.

1.2 Overview

Since their discovery, polymers have rapidly become an important part of everyday lives and have diverse applications ranging from plastic bags to bullet proof clothing. The reason that their applications are so many and so varied is because polymers themselves can be tailored by their chemistry and processing conditions to have the desired macroscopic properties. Polymers derive much of their properties from being a long flexible chain, or a complex architecture of several long flexible chains. This

has lead to many interesting and insightful models, based on the fundamental concept of long flexible chains, being used for explaining and predicting polymer properties.

As polymers have been discovered relatively recently, the development of physical models has been greatly aided by modern computational efforts. This condition has lead to a rapidly growing field of computer simulation evolving hand-in-hand with experimental investigations.

The method used in this study is focused on polymer systems which are derived from conditions where inter-chain interactions, or entanglement interactions, dominate the mechanical response. A common system where this occurs is a molten sample of a highly entangled polymer with high molecular weight. Under the right conditions these entanglement interactions lead to elastic behavior over laboratory time scales. Another polymer system with soft elastic behavior is a cross-linked network. Both highly entangled melts and polymer networks have behaviors suggestive of a network of deformable springs, and both theories and simulation models have been proposed based on this concept.

An additional polymer phenomena relevant to this study is the three distinct phases a polymer can experience; molten, crystalline, and glassy states. Whether a polymer is above or below its glass transition temperature, and the degree to which, if any, the polymer is crystalline can determine whether the polymer exhibits a high modulus and brittle properties or highly extensible, ductile properties, or other unique properties. In fact, there are systems in nature, such as spider-silk, which use a combination of crystalline and entangled soft polymer regions to help achieve highly desirable

mechanical properties[1-2]. Additionally, synthetic systems such as nylon have been discovered in search of similar mechanical properties[3].

Coarse-graining is a technique commonly applied to polymer simulation to increase the feasibility of simulating large or complex systems. The amount of coarse-graining required to simulate a phenomena of interest reflects the complexity of the system and the size and time-scale of interest. One class of simulation model uses a level of coarse-graining based on the entanglement spacing of the molten polymer counterpart, and is represented by an entanglement network (Figure 1). This class of simulation can also use a Kinetic Monte Carlo algorithm to describe their dynamic behavior enabling timescales on the order of system failure to be modeled, as is done in the TBM and DCM.

Traditionally polymer simulation belongs to one of two isolated fields, continuum and molecular level modeling. Continuum level modeling had the ability to model system sizes and time scales relevant to polymer processing, and molecular level modeling specialized in understanding subtle differences in polymers arising from the molecular level chemistry. Now, there are strong efforts to bring molecular level details to continuum modeling, as well as scaling up the systems sizes that can be addressed by molecular simulation. This has created a field in itself, commonly referred to as multi-scale modeling or meso-scale modeling.

The method used in this study is a meso-scale technique based on the entanglement network framework. The following section is a review of the TBM, which is work that introduces these concepts.

1.3 Temporary Bond Model

Smith and Termonia [4-8] developed a two-dimensional representation of an entanglement network and focused their study on the stress-strain relationship of polyethylene (PE). Their study showed promising results while testing a variety of experimental variables including molecular weight, entanglement molecular weight, strain rate, and temperature. Their model introduces the temporary bond (Figure 1), which they claimed accurately reproduced a semi-crystalline stress response of polyethylene. Sample morphologies also show similarities to experimental systems[6]. These studies relied on a lateral affine assumption, which fixes the entanglement points in the lateral dimension to conserve simulation sample area.

The TBM introduces a Kinetic Monte Carlo (KMC) framework for handling the dynamics of entanglement slippage and temporary bond breakage. This technique provides a computationally feasible path to simulating long time scales. In the case of entanglement slippage, it is reasonable to expect molecular level insight into systems that are dominated by polymer entanglement, such as melts experiencing reptative dynamics.

A promising extension of entangled polymer simulations is the application to more complex systems, including systems with heterogeneous microstructure, free surfaces, or networks with novel architectures. Microstructure can be explicitly included to help interpret the behavior of novel systems such as spider-silk [1-2]. Additionally, with the incorporation of accurate surface free energy to entanglement network

simulations, systems such as fibril formation of adhesive interfaces could be studied.

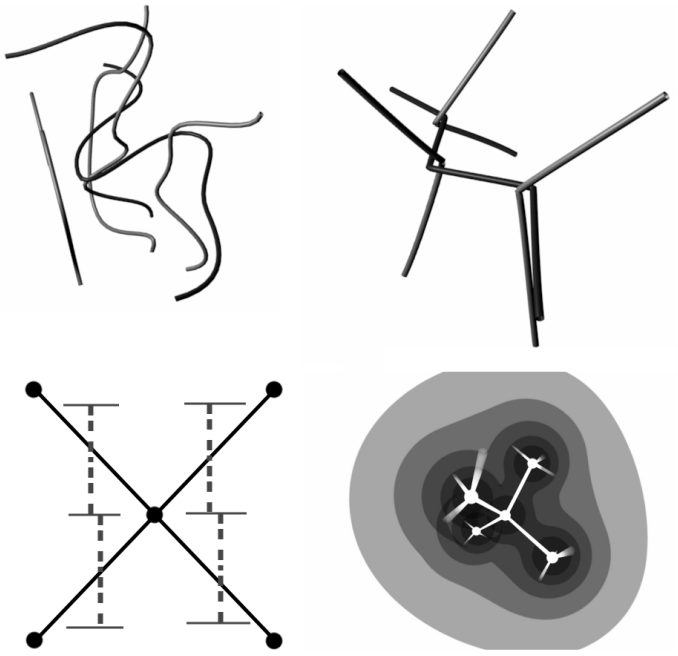

Figure 1: Schematic representation of the frameworks for the coarse-grained models. Above is a representation of entangled polymer and its reduction to primitive paths between entanglement points. Below are the schematic representations of the TBM and the DCM. The TBM is two dimensional, spatially uniform, and has linear elastic temporary bonds (dashed lines) acting between all of its segments. The DCM is naturally three dimensional and uses overlapping density clouds to represent monomer units of each coarse-grained polymer segment.

The pioneering work on the TBM [4-8] involved a series of comparisons between experiments and the mesoscopic model for which the variation of a experimental condition yielded qualitative and at times semi-quantitative agreement with the TBM. The polymer system of these studies was linear polyethylene.

The first of this work focused on the effect of molecular weight [4]. In this case the higher molecular weight directly leads to more entanglements per polymer chain and a lower concentration of chain ends in the entanglement network. All reported systems have an initial linear region of stress response. This region has the modulus of the value selected for that of the temporary bonds, 4MPa. This linear region ends at a yield point, characterized by a sharp drop in the stress response, which is due to the beginning of temporary bond breakage. When the first bond breaks, a cooperative loading of neighboring bonds leads to heightened temporary bond breakages in the immediate vicinity. The response of the different molecular weight systems beyond this strain is very different.

The reported molecular weights (1900, 9500, and 250,000) were chosen to display the different stress responses due to characteristically different fracture behavior. The low molecular weight system has brittle fracture, where the temporary bonds along a horizontal section (strain is applied "vertically") of the sample broke with few or no chain segments bridging the temporary bond fracture zone. The middle molecular weight sample showed a formation of a neck; that is, a horizontal region of broken temporary bonds with high local strain, that grew steadily through the draw region of the stress response. Finally, in the high molecular weight case the deformation is spatially uniform, with the temporary bond breakages occurring throughout the sample but not leading to necking behavior. The morphology of an additional simulation with MW=20000, omitted from the stress comparison, was displayed and described to have multiple necks forming and growing as in the single neck case.

In the molecular weight study, only the intermediate molecular weight system was

affected by activation of entanglement slippage. Simulations with and without slippage implementation were reported and show characteristic differences. In the case with slippage occurring, a dramatic hardening at high strains due to the finite extensibility of the chain segments was offset by their ability to slip through entanglement to relax the segments of high strain. This leads to a prolonged drawing region and a higher maximum draw ratio. The effect of slippage was undetectable in the other cases of low and high molecular weight. The conclusions of this study focused on the interplay of the concentration of chain ends and how it leads to load transfer and the resulting patterns of temporary bond breakage. Additionally slippage was shown to have a significant effect in some instances, something that would be explored in later studies by same authors [5-8].

The molecular weight study was shortly followed by a study of the effect of entanglement spacing on the stress response of the TBM [5]. An experimental comparison was made possible by diluting a polymer with a solvent prior to crystallization. This study would make comparisons to solution-crystallized thin films of Ultra-High Molecular Weight (UHMW) polyethylene, in both stress response and morphological characteristics. Simulation and experiments agreed with a dramatic effect on the post-yield strain hardening as well as the strain at break. The observed trend is that a higher entanglement spacing leads to a longer draw region and a higher maximum strain. This is in part because the longer chain segments between entanglement points can stretch farther, from a random coil configuration to a fully stretched one, once the accompanying temporary bond is broken. The trend continues until the entanglement network has a high enough concentration of chain ends relative to entanglement points, that brittle fracture occurs. This is analogous to the response

of the low molecular weight study from earlier.

The entanglement spacing study involved four different entanglement spacings, each simulated at two temperatures (109 ºC and 130 ºC) [5]. Slippage has no effect in the low temperature case. To investigate further, a power law was fit to data relating maximum elongation to entanglement spacing. The simulations result in a exponent of -1/2, which was in conflict with another study from around that time [9]. The prefactor of this relation can be shown to be 6.5 for the case when no slippage is occurring which is consistent with the simulations at temperatures of 109ºC which results in a prefactor value of 6.4. However; at the simulation temperature of 130ºC slippage is affecting the maximum draw ratio, with the prefactor from fitting the set of entanglement spacing simulations to the power-law trend is significantly higher.

When comparing the morphologies of the TBM simulation to micrographs of the strained UHMW polyethylene films, four noticeably different morphologies occur consistently between simulation and experiments. Although simulation size scales are smaller (~μm) than those of the experimental micrographs (0.1mm) [5], the resemblance is a promising result in support of the ability of this type of model to incorporate molecular details to predict macroscopic deformation properties.

Based on the temperature dependent description of the slippage and temporary bond breakage, it can be expected that the simulation parameters of temperature and strain rate will have similar effects on the stress response. This is largely confirmed by the model authors as they study these effect independently [5]. Again this study was compared to an experimental system of polyethylene, and the authors report semi-

quantitative agreement to the experimental system for the maximum draw ratio.

A following study [6] reported the stress response of the simulated system over several temperatures at a single strain rate and over several strain rates at a single temperature. The focus of the comparison to experiments was with the maximum draw ratio. The polyethylene system has a draw ratio at failure that is sensitive to both temperature and strain rate and a maximum in this property is observed over the range of systems studied. This maximum has significant importance when considering tailored applications for polymers. The simulation system used a monodisperse molecular weight of 143000, and the experimental polymer was supplied as close to mono disperse with molecular weight of 125000, and a semi-quantitative agreement was achieved.

The trends observed supported the close relationship between rate of strain and temperature, in that they both invoke the same trends. Decreasing the elongation rate is analogous to increasing the temperature. This is intuitive as raising the temperature will directly raise the rate of kinetic events which is equivalent to reducing the strain rate which will allow more time for the kinetic events to occur.

The behavior of the stress response shows a drastic effect on the deformation hardening, in the region beyond the yield point. At high strain rates or low temperatures this hardening is clearly present and then subsides, in effect "making way" for the increase of the maximum draw ratio. Beyond the maximum, at low strain rates and high temperatures, temporary bond breakage and slippage occur to an extent that the failure occurs at a low strain. An interesting interpretation of this behavior is

that an increased temperature can prevent catastrophic failure by "smoothing out" the deformation hardening. This occurs directly through slippage leading to disentanglement of two polymers, which is suppressed at lower temperatures.

The optimum temperature and strain conditions for the studied systems results in a maximum draw ratio of 23, in agreement with the experimental system. However; the conditions themselves, temperature and strain rate at optimal terminal strain, do not agree as well. The authors propose that the model parameters U (activation energy of slippage) or equivalently β (slippage volume) could be used as fitting parameters to obtain better agreement.

A final trend reported in this study[6] was the trend of optimum drawing temperature based on the molecular weight. This involved simulating a series of different molecular weights (~10^4 to 10^5) each under a series of temperatures to find the optimal condition. The trend was reported to be in agreement with experimental observation and followed a linear trend of optimal temperature to the logarithm of molecular weight. The increase in the optimal drawing temperature with increasing molecular weight can be explained by the needed increase in slippage to accommodate the lower concentration of chain ends available to slip.

The TBM prevents a comparison of initial modulus upon changing temperature and strain-rate, it has a constant parameter of K_{vdw}, the modulus of the temporary bonds. This fixes the initial modulus as constant.

The earlier publications from the TBM series [5-6] reported trends based on molecular

weight of the PE system, but these studies used a monodisperse molecular weight distribution, which are not always available experimentally. Many of the properties reported were expected to have an averaging of properties when considering a distribution of polymer molecular weights. The next paper in the series [7] was dedicated to studying the effect of polydispersity of the linear polyethylene system. When considering the maximum drawability from previous studies [6], one would expect that property to be sensitive to the higher moments of molecular weight, and not just the average molecular weight. The authors report that no systematic correlation of the number average molecular weight and maximum drawability is observed. It had been shown elsewhere [10] that log normal MW distributions are correlated to maximum draw ratio, and accordingly the TBM simulations were studied under varying conditions of polydispersity ratio M_z/M_w and the M_t average molecular weight from Graessley[10].

A general trend was observed, where a decrease in maximum draw ratio and a broadening of the window of optimal drawability resulted from an increase in polydispersity. Stated another way, to reach a high maximum draw ratio, having low polydispersity can compensate for a lower molecular weight. Experimental evidence was provided to show a qualitative agreement of simulation and experiments. The authors were careful to note that when reporting the clear dependence of maximum draw ratio on both average MW and polydispersity the trend is not uniquely defined by just these variables. They argue that for high polydispersity ratio M_z/M_w it is likely that higher moments control the optimal drawability.

To illustrate the dependence on higher order moments of molecular weight the authors

choose to study a system of a bimodal blends of low and high molecular weight polyethylene (M_1=6240 and M_2=148200), each of the components being near monodisperse. The motivation for this selection was the observation of bimodal distributions in polymer networks leading to interesting properties [11]. A highly non-linear relationship between composition of blend and maximum draw ratio was found. The study found a local maximum in maximum draw ratio at the composition of 50/50 weight percent.

The analogous relationships of both temperature and strain rate to the optimal draw ratio was also explored. It was proposed that under some conditions blending may be used to reduce the temperature of maximum drawability to below the melting point for commercially interesting polymers.

The final paper by Termonia and Smith in the series on the TBM deals with the effect of temperature on orientation efficiency [8]. This study was motivated by earlier work, on a two state model, involving one of the authors [12-13], which aimed to account for the relationship of draw-ratio to modulus for a broad range of polymer systems. That work captured some essential behavior but assumes macroscopically affine deformation, which was used to explain disagreement with experiments at elevated temperatures [14-15].

The two state model [12-13] involved treating a chain segment as a coil and helix element, decoupling the moduli of the polymer segments in the strain direction and in the direction orthogonal to the strain direction. This treatment was a natural fit for a simulation methodology which microscopically tracked chain segments, like the TBM.

In fact, this pairing comes with the added benefit of being able to apply the two state model to each element individually, and avoids the need to assume microscopically uniform deformation. The coil-helix element is assumed to take the place of the temporary bond element. Another addition is made to this version of the TBM; chain re-entanglement is allowed to occur through two possible scenarios. Firstly, two interpenetrating chain ends may re-entangle with one another provided their number of segments are both greater than the average number of segments at the starting condition. The second scenario is a re-entanglement of a chain end with another chain segment (not a chain end) provided the center point of the chain segment is within the radius of gyration of the chain end. Combined with slippage this will set up a relationship of disentanglement due to slippage out and the formation of new entanglement points.

The authors report that the TBM without slippage matches the original two-state model as the TBM without slippage or temporary bond breakage was known to result in affine deformation. However, with slippage a reduction of the modulus at high draw ratio is observed due to the disentanglement and then redistribution of entanglements that are not oriented due to strain. The temperature dependence of this phenomenon is reported and the authors observe that there is a critical temperature above which the reduction in moduli at high strain is large. The increasing temperature directly increases the kinetic process of slippage which accounts for the reduction in moduli. They compare the model predictions, for this maximum temperature where tensile deformation is efficient, to experimental observations for a range of molecular weights (ranging from 10^5 to 10^7). Again, the authors propose fitting of the slippage parameters to achieve quantitative agreement, but that was

beyond their intentions with the study [8].

Termonia continued to study similar systems including composites [16-20], and network systems [21-22] along the lines of the initial configuration procedure of the TBM. The TBM would go on to inspire others to study similar computer models.

In addition to inspiring the DCM which will be covered later, Termonia's kinetic model was adopted by others in a more similar form. Bicerano et. al. used a similar model with the goal of predicting stress-strain curves of a range of different amorphous and semicrystalline elastomers [23]. Significant changes were made to the model. Firstly, the formation of the initial condition involved an algorithm to alter the connectivity of the polymer chains on the densely packed grid. This algorithm seeks to explore the phase space of chains on a densely packed grid to alleviate some the issues brought up in Mansfield's [24] criticism of the forward seeking algorithm. The other major change is a more intricate morphology of crystalline links and tie chain links as apposed to uniformly distributed temporary bonds used by Termonia. These authors use a conjugate gradient method for relaxing the entanglement network, as opposed to the block relaxation method of Termonia. They implement the lateral affine assumption and slippage as in the original model.

An important improvement of this model is that crystallinity is accounted for in an explicit manner, through the crystalline links and tie chain links. This version of the TBM can more directly account for different morphologies of the starting condition. To specify the starting morphology these simulation accept parameters for the percentage of junctions that are crosslinks, volume percent crystallinity, crystal size,

and a force constant for the crystalline links.

The authors find a good general agreement to an impressive range of polymer systems simulated but fall short in achieving quantitative accuracy. They report that the more complex semicrystalline version was less accurate, and the author's attribute this to simplifications they were forced to make to reduce computer time, as well as being the target of future study.

More recently Reddy et. al. have revisited the Termonia and Smith model [25]. They conduct an extensive parametric study of the original TBM, including the slippage parameters which were not modified in the original author's publications. They also report the stress decoupled into its components, whether they be elastic entropy spring contributions or the loading the temporary bonds and use this to describe the observed semicrystalline stress response.

The algorithm used to generate the initial condition used in the TBM [4] was similar to other Monte Carlo studies which were going on at the time [26-30]. These studies focus on the phase transitions in polymers on a two-dimensional lattice. Later, Mansfield [24] found that a three dimensional system undergoes an order-disorder transition that is first-order, but for a two-dimensional system the transition is second-order and critical. In addition to these findings the author also provides a critical analysis of the scanning technique, used by Termonia, which was noted by Bicerano et. al. [23] and used as grounds to introduce a different technique for generating the initial condition for their version of the TBM.

1.4 Density Cloud Model

The density cloud model (DCM) was introduced as part of a study to address the mechanical reinforcement via *in situ* copolymerization of an immiscible polypropylene and polyamide (PP/PA6) system [31-33]. The study involved i) creating a theoretical expression for grafted and free polypropylene densities away from the polyamide interface [31], ii) generating an explicit entanglement network consistent with this result [32], and iii) deforming the entanglement network using the DCM which does not use any fitting parameters [33].

Work had been conducted on improving the fracture strength of immiscible polymer/polymer interfaces [34-36], via the compatibilizing of polymers via an *in situ* reaction of the two polymers creating a diblock copolymer at the interface. To study this system, it was desired to have a theoretical treatment which uses a hierarchical approach [31]. Parameters used in the study would be from the experimentally determined values for the system of PP/PA6 compatibilized with the reaction product between PP-*g*_MA (maleic anhydride-grafted PP) and PA6, of which experimental studies existed [37-39]. The hierarchical coarse-grained simulation approach is appropriate because the fracture properties of the composite system are believed to be directly related to entanglements [31].

In order to generate entanglement networks representative of an interface, an interface with grafted and free PP chains was modeled using the self-consistent field (SCF) theory [31]. The resulting grafted and free chain profiles could be used to help generate an explicit entanglement network. The grafted and free PP chain system is

appropriate considering the experimental system modeled. The compatibilized interface is formed by clamping sheets together and reacting the compatibilizer at a temperature above melting temp of PP but below PA6 [38-39]. The temperature and time of this reaction control amount of grafted chains, and the reaction is believed to be limited by the diffusion of PP to interface [39]. For this reason the theoretical study treats the PA6 phase as an impenetrable wall, and the affect of grafting density is studied [31].

The SCF theory was originally published by Scheutjens and Fleer [40-42]. The original theory was extended to combining methods from earlier studies[43-47], and a multicomponent SCF model with stiffness effects was used for the system with free and grafted chains at the interface [31]. The authors point out that semicrystallinity is ignored like the TBM study of Termonia [4], and state a future goal of incorporating the crystallinity of the PP phase.

Literature parameters, such as volume fraction and bond order parameters were used to calculate the polymer species profiles [31]. A systematic study was conducted for influence of molecular weight distribution of grafted and free chains and surface density of the grafted chains on the structure of the interface. It was concluded that the effect of MW distribution of grafted chains on structure is much greater than that of the free PP chains. It was also found that for realistic systems (matching MW distribution of grafted and free chains to experimental studies) the grafted chains are significantly stretched, transitioning from a random coil to brush configuration at small grafting densities. It was noted that for the systems studied, some free chains penetrate to the interface at realistic grafting densities, and the amount is sensitive to

the graft density. Additionally, with close to monodisperse systems, a maximum in region length where grafted and free chains intermingle is observed. Alternatively, for polydisperse systems this region rises to an asymptote with increase surface density of grafted chains.

The second step of the hierarchical approach is to generate an explicit entanglement network, by placing entanglement points of polymer chains in continuous three dimensional space [32]. The positions of chain ends and entanglement points conform to the density and conformation distributions given by the SCF model of interface or PA6, PP, and compatibilizer, as follows. For a given polymer chain, entanglements are placed along its contour at a separation equal to the entanglement molecular weight from experimental studies [48-49]. Polymer entanglements are placed based on the statistical weights for grafted and free chains from the SCF results from their previous study [31]. Although the initial placement also follows Gaussian statistics, with respect to relative stretch, the entanglement points are not in mechanical equilibrium. To equilibrate the system, a random rearrangement of entanglement points is conducted without perturbing entanglements lateral placement from the interface.

This method was successful at generating an explicit entanglement network , as desired [32]. The configurational and conformational profiles (i.e. free or grafted polymer profiles and degree of stretching) are consistent with the SCF predictions. From the explicit entanglement network, it can be calculated the number of entanglement points between one grafted and one free chain. For a monodisperse MW system studied, a maximum of such entanglements occurs with respect to grafting

density, leading to a prediction of optimal surface density for experimental systems. Alternatively for polydisperse free chain MW systems, a plateau value for the amount of free-grafted entanglements is observed. An increase in entanglements between free and grafted chains is found in response to an increase in surface density of grafted chains. This behavior is in agreement with the trend of the region of interpenetrating free and grafted chain from the earlier SCF study [31]. The authors point out, that although this method is successful at generating an explicit entanglement network consistent with SCF results, at the time of publishing new information about entanglement distributions along chains was already underway [50-53].

The third and final step of the hierarchical approach is to deform the entanglement network and observe the mechanical response up to and through the fracture process [33]. The density cloud model (DCM) used for the deformation is a coarse-grained approach as apposed to direct Monte Carlo or Molecular Dynamics, such as the Monte Carlo bond-fluctuation model study that had already been conducted [54-55]. Terzis, Theodorou and Stroeks [33] created the DCM for the large scale deformation of a semicrystalline PP system, inspired by the Temporary Bond Model (TBM) for PE [4]. A valuable improvement in this model was incorporating the details of the monomer units of a segment between entanglement points as a density cloud (Figure 1). This made calculating the free energy of the entanglement network an integration over simulation space and dependent on more than a linear combination of functions of neighboring bond vectors. Additionally, the Density Cloud Model (DCM) allows for the relaxation of all degrees of freedom of the entanglement points and circumvents the need for the lateral affine assumption. The density clouds represent an average of all possible configurations of the chain with known end-points in space. These added

details come at the cost of a more computationally expensive calculation of free energy of the entanglement network. The authors of this model have used it to study the failure of an adhesive interface, but did not compare it directly to the TBM.

The DCM of Terzis et. al. used a MC integration of and ideal chain to generate the density clouds used in the simulation. Earlier work by some of the same authors explored an alternative method to calculate such systems, including those with more complexity, such as diblock copolymer chains [46]. The goal is to have a representation of all possible monomer units of an ideal chain where they are likely to be located when both ends are tethered to a certain position.

The deformation of the entanglement network under the DCM leads to fracture in the intermingling region of free and grafted chains [33]. The Young's modulus of the PP/ PA6 compatibilized interface is approximated to be 0.49GPa, smaller by a factor of two from experimental studies [56-59]. Additionally, the deforming system experiences a yield point when chain rupture is occurring at a significant rate and a reduction in stress results. This is in contrast to the yield point of the TBM resulting from breakages of the temporary bonds only [4]. This deformation model concludes the simulation methodology that relies only on experimentally know parameters, and presents a roadmap for studying microscopic effects on macroscopic properties.

1.5 Polymer Network Theories

Polymer Network theories have developed over many years, and recently the Non-Affine Slip-Tube (NAST) model combining ideas of earlier models has predicted a

universal behavior for polymer networks in tensile experiments[60]. This model and earlier models are based upon an effective chain picture of a single network strand connected to a deforming background. All possible arrangements and connectivity of the effective strands are incorporated into the theory's prediction of the stress response. The simplest model is the affine network model where the effective chain is simply a Gaussian chain anchored in the affinely deforming background. The ideas of later models that were incorporated into the NAST model are: fluctuations of the network chains end points represented by a virtual chain attaching the network chain to the deforming background; entanglement effects represented by additional virtual chains located at distinct points along the network strand; and the ability of virtual strands representing entanglements to slide along the contour of the network strand. The virtual chains are not Gaussian chains, but have a force response that is changing to represent the deformation of the confinement tube a network strand belongs to.

The basic idea behind network theories is to translate the microscopic deformation of an individual network chain into a collective macroscopic response. Mathematically, this involves treating an effective network chain, and considering all possible ways of internally connecting the network strands, while having some strands connected to the boundaries of the system. This is done by evaluating the end-to-end vector correlation function, the statistical average of the product of two segment vectors. The expression for the end-to-end correlation function changes based on the formulations of the model.

All the network theories described here rely on the Gaussian approximation for the polymer segments to readily describe, mathematically, the thermodynamics of

stretching such a segment. Several models have been proposed, and they differ based on how they treat an effective network strand. They vary in how the anchor points of the network strand are allowed to fluctuate and how intersegment interactions, or entanglement effects, are introduced.

The first model to describe polymer network behavior is the affine network model [61-62], the theory which introduced the connection between the molecular description and the deformation properties of a network. No entanglement effects enter this model so the effective network chain is simply the linear polymer chain whose ends are at two crosslink points. These crosslink points are embedded in the affinely deforming elastic background. By evaluating the end-to-end correlation function of this model, the classical affine network result is recovered.

The model description of the affine network model serves as the foundation for all the other network theories. Additionally, the tensile and compressive stress response of this theory is the basis for comparison of these theories and network stress responses are commonly reported as a reduced stress, normalized to the affine theory result, known as the Mooney ratio [63-65].

The first model to build upon the affine network model was the phantom network model [66-67]. The main addition to this model is that the crosslink points at the end of the effective chains were not embedded in the elastic background but were allowed to fluctuate. This provides a more consistent picture to a real network crosslink which would be undergoing thermal fluctuations. Expressions for this model have been derived generally for different functionalities of the crosslink junction [68]. It has

been pointed out [60] that the phantom network model is equivalent to a combined chain of the network chain and virtual chains tethering the crosslinks to the affine background. In this equivalent description the amplitude of fluctuations are controlled by another Gaussian chain, or virtual chain, which is itself embedded in the affine background. Deriving the result of the phantom network model from either representation yields the same result for the network stress. The functional form of the elastic stress is the same for the affine model and the phantom network model. The expressions differ only by a prefactor.

Later, the constrained network model introduced the idea of non-affine tethering of network crosslinks. Instead of having a harmonic potential confining the crosslinks that does not change with the deformation, the potential deforms with the macroscopic deformation. As the elongation in the strain direction becomes large, the fluctuations in that dimension deform similarly. This interaction is accomplished by a non-constant and also non-linear expression for the virtual chains number of segments in any of the principle directions, with respect to the elongation in that dimension. When formulated in the correct way, these confining virtual chains only affect the end-to-end distribution function of the chains and do not directly contribute to the elastic stress. This model was first solved using an approximation [69-70], which was used in later generalizations [71-72], and only recently [60] solved exactly. The approximate solution captures qualitatively the results but deviates by up to 20% in certain regions of the stress response [60].

It is clear that an accurate description of a network chain needs to incorporate topological constraints, and this is a focus of modern network models. These models

involve adding additional constraints along the network chain which reduce the conformations the chain can take. Klocszkowski et. al.[73] proposed a diffused-constraint model in attempts to have the confining effects on all points along the network chain, not just at the crosslinks. This constraint was averaged over all possible locations along the network chain, and thus was allowed to "diffuse" along the chain. Rubinstein and Panyukov [60] point out that this method ignores the connectivity of the chains and thus the correlations between connected fluctuations, and thus ignores an important aspect of being an polymer network. They also provide an approximate solution to this model [60].

Early work by Edwards [74] introduced the concept that a polymer was surrounded by topological constraints which can collectively be thought of as confining the single chain to a tube. This idea has been appropriately dubbed the Edwards Tube Model. Mathematically this model consists of a potential acting on each monomer of the polymer chain. This potential, or equivalently the tethering virtual chain embedded in the elastic background, does not deform with the macroscopic deformation as in other later models.

From the tube model one can develop an expression for the tube diameter, which is an approximate measure of where the monomers of the chain will lie along the center line of the chain. This tube diameter is a non-linear expression dependent upon the length of a monomer unit and the number of monomer units between the topological constraints.

Rubinstein and Panyukov [60] point out some limitations of the Edwards tube model.

Firstly, from the microscopic definition of stress the virtual chains will directly contribute to the stress of deformation, something that is not consistent with the fundamentals of the model. The stress of the system should be described solely by the elastic contributions of the real chains and the topological effects should be independent of strain. Secondly, the Edwards tube model predicts a strain independent Mooney ratio, like the affine and phantom network models, something that is not observed experimentally.

An important development in polymer network theories involved the combination of two existing ideas, when Rubinstein and Panyukov [75-76,60] added deforming topological constraints to the Edwards tube model. The deforming constraint was taken directly from the constrained junction model, but now this non-affine constraint was applied to each monomer along the tube as laid out in the Edward's Tube model, with some subtle differences. Tethering chains are attached differently than in the Edwards tube model. Instead of being attached along the center line of the chain, they are attached randomly in space to ensure Gaussian statistics at the starting condition.

From the model formulation, one can deduce that in the highly entangled limit $N>>N_e$, the behavior of the non-affine tube model is equivalent to the constrained junction model with a functionality of 2. A direct result of the non-affine tethering is that the tube diameter is changing similarly with the network deformation, a result that had also been obtained by others [77-78].

The non-affine tube model was compared to experiments [79] and captured some of the behavior of the real system. This is evident when comparing the Mooney ratio of

the model and experiment and realizing they share some features. However, this model would later be improved upon by its authors to provide an even better description of the experimental behavior. The resulting expression for the network stress is a two parameter expression, and those parameters are the crosslink and entanglement moduli, with the crosslink modulus equal to the modulus of the affine system without entanglements, and the entanglements contributing the non-affine effects to the stress response through the entanglement modulus.

The concept of a slip-link was introduced in the context of polymer network theories by Edwards et. al. [80-82], which formed the basis for being later incorporated into Brownian Dynamics simulations and Entanglement Network simulations. The concept is that polymer entanglements arise from two segments of polymer chains inability to pass through one another. This behavior can be approximated by a point at which the two chains coincide and segments of the same polymer chain may move from one side of the slip-link to the other side. Mathematically, this situation can be described and total number of slip-links is expected to be given as a parameter of the theory, or derived form the plateau modulus of the network system. The results of these models gave correct limiting behavior and agreement with experiments; however, the later theories of Rubinstein and Panyukov treated entanglements in a different fashion, as a single network chain with a virtual chain attached to the deforming background.

In 2002, a network theory was proposed [60] that shows an impressive matching to a large range of polymer network experiments, and seems to capture the universal behavior of such systems. The Non-Affine Slip-Tube (NAST) theory, builds directly

on the authors' earlier work with the Non-Affine Tube Theory. Tethering virtual chains are allowed to move along the chain, as if they were rings instead of permanently attached, which is a consistent representation of the topological constraints ability to slip by one another. While a slip-link involved two network chains, the topological constraints in the slip-tube model are a virtual slip ring attached at one end to the network chain and on the other end, embedded in the elastic background (i.e. the slip-link involves two network strands and the slipping element of the slip-tube theory involves one network strand and one virtual chain).

The slippage elements of this theory can slide along the network chain but cannot pass through each other. The authors show that in the limit when each monomer has a slip-link, the result is non-affine tube behavior, since the slippage elements cannot pass through each other. Conversely, when the slip links are separated by the entanglement molecular weight, the fluctuations are of the same size as the Gaussian stretch distance of the entire network strand and no confining tube is established. The added degrees of freedom of the slippage alter the stress response expression, through the denominator in the term for the entanglement contribution to the stress.

The effect of this slippage is to relax highly strained network segments by allowing some monomers to slip from other parts of the chain which are aligned in a less extended dimension. This is an additional degree of freedom when considering all possible conformations of the network.

Rubinstein and Panyukov solve the slip-tube model and present a universal plot of experimental data [65,83-84,79] fitted to the slip-tube result [60]. This involves fitting

two parameters, the cross-link modulus and the entanglement modulus. The crosslink modulus has a direct analogue to the contribution of an affine network if the entanglements were to be turned off, and the entanglement modulus is a measure of how much non-affine behavior arises due to topological constraints.

1.6 Molecular Simulation Techniques for Entangled Polymer Systems

Explicit simulation of individual polymer molecules enables the highest level of molecular insight. Molecular simulation techniques such as molecular dynamics and bond fluctuation Monte Carlo offer a clear picture of individual polymer chains, while simultaneous allowing for the approximation of bulk macroscopic properties. These techniques have been applied to all types of polymer systems, from dilute polymers to dense polymer systems and complex composite systems. Following is the review of some work most relevant to the entanglement network model framework.

Monte Carlo simulation has proven to be an effective tool for understanding the thermodynamics of polymer systems. The tensile response of end-linked polymer networks have been studied using the bond fluctuation model [85-86]. In these studies the topological interactions of the polymer chains are handled via the excluded volume interactions of the coarse-grained polymer representations. The network topology is generated using a Monte Carlo technique to mimic the end-linking chemical reaction of experimental counterparts. This molecular simulation framework allows for the study of how microscopic effects such as chain stiffness affect the macroscopic stress response. A model system of an entanglement-free network was also studied and found to have peculiar stress response similar to other complex biological systems

[87]. Other studies have used similar approaches including the simulation of a network of helix polymers [88-89].

Atomistic simulations of polymer networks are also possible through conventional molecular dynamics simulation. This technique helped establish the importance of trapped entanglements [90-91]. More recently Grest et. al. [92] has used atomistic simulation to shed light on a previous observation of inter-chain interactions dominating the microscopic stress of dense polymer systems [93-94]. With a careful presentation of the non-linear stress response of polymer networks, the authors were able to present scaling relationships and arguments to the feasibility of existing network models, as well as comparing to experimental studies using end-linked networks [95-96].

Additionally, nonequilibrium molecular dynamics can be used to study polymer systems, such as was done by Kroger et. al. in investigating the crossover molecular weight of polymer melts [97].

A simulation method used to compare with network models, and account for discrepancies between model and theory, is primitive chain network simulations [98-109]. This method is based on Brownian dynamics and can incorporate ideas such as tube length fluctuations, and thermal and convective constraint release, with the added benefit of explicitly accounting for topological interactions through entanglement points. This topological treatment is in contrast to the mean-field treatment of these interactions in theories [110-120]. The primitive chain network simulations consists of a three-dimensional network of polymer segments between

tetra-functional slip-links. Chain sliding through slip-links is incorporated into the stochastic equations of motion, and the distribution of overall network conformations are solved as in conventional Brownian dynamics.

Recently, a method of generating an entanglement network from an atomistic description of a polymer melt has been proposed, called Primitive Path Analysis (PPA) [50-51]. This method produces the primitive path for each polymer chain, a concept originally proposed by Doi and Edwards [112]. In this method, an equilibrated polymer melt is simulated with modified atomistic potentials. The end points of the chains are not allowed to move and the new atomistic potentials drive the chains to completely collapse, except that they are prevented from crossing other chain segments. The results are segments of the chain arranged linearly between points of uncrossibility which represent the primitive entanglement mesh. This method was compared to an analytical expression for the primitive path length [121], and has inspired Brownian dynamics studies to correlate primitive path parameters to a polymer's viscoelastic response [122-124].

Similarly, Tzoumanekas et. al. used a Monte Carlo method of producing a primitive path [52-53]. In this method a new Monte Carlo move is introduced which attempts to straighten, by arranging linearly in space, a variable size region of the polymer. The move is not allowed to lead to the centerline of chains crossing one another. The result is analogous to the molecular dynamics method of PPA.

CHAPTER 2

TEMPORARY BOND AND DENSITY CLOUD MODEL COMPARISON

2.1 Introduction

The two dimensional Temporary Bond Model (TBM) and fully three dimensional Density Cloud Model (DCM) share many similarities, but have yet to be applied to the same polymer system for direct comparison. A primary objective of the current study is to understand the fundamental units of coarse-grained simulation, including the temporary bond and the density cloud treatment for excluded volume. To study this, the TBM will be extended to three dimensions so that identical starting conditions can be shared between it and the DCM. To simulate analogous systems, the DCM is carefully studied with respect to minimizing numerical affects associated with the numerical integration of the density clouds.

The two models are compared directly using the system simulated in the original publication of the TBM [4], but in three-dimensions.

2.2 Simulation Models

Both the TBM and the DCM rely on an entanglement network and keep track of the evolution of the entanglement points through the course of the simulation. Polymer contours are accounted for, because a single polymer molecule will connect several entanglement points. In this manner the entanglement effects of the polymer molecules are concentrated at tetra-functional entanglement points which represent

two participating strands which cannot cross.

The primary component of the entanglement network is the segment of polymer tethered between entanglement points. The concept of an ideal chain held at a certain stretch amount is well studied and the entropy spring representation of the following form is used to model the contributing force of the polymer chains between entanglement points.

$$F = \frac{k_B T}{l} L^* \left(\frac{r}{nl} \right) \tag{2.1}$$

In the expression above k_B is Boltzmann's constant, T is temperature, r is the segments stretched distance, n is the number of monomers of the ideal chain and l is the monomer length. This study uses the Pade approximation to the inverse Langevin equation.

$$L^*_{pade}(x) = \frac{x\left(3 - x^2\right)}{1 - x^2} \tag{2.2}$$

As in the original formulation [4], the temporary bonds are present uniformly and completely between neighboring entanglement points (Figure 1) at the start of a simulation and break according to Transition State Theory. The mechanical response of the temporary bonds is linear and serves as the primary component of the initial modulus, since the entropy spring contributions are small in the initial unstretched regions. It is important to note that the temporary bond does not align with the vector between entanglement points but responds to the component of deformation in the strain dimension (ε_y in the equation below).

$$\sigma_y = K \epsilon_y \tag{2.3}$$

Alternatively, the DCM accounts for all configurations of polymer segments in the entanglement network, represented in an averaged way by the polymer density clouds. The density cloud represents all possible configurations of an ideal chain tethered at ends according to where its terminal entanglement points lie. The authors proposed accurately generating the density clouds using Monte Carlo simulation of ideal chains. In our study the density clouds are Gaussian density clouds to ensure that they are smooth and well behaved, and can be generated from the following equation.

$$P\left(\vec{R}, \vec{R_{e1}}, \vec{R_{e2}}, N_e\right) = \sum_{n=1}^{N_e} \frac{P\left(\vec{R_{e1}}; n\right) P\left(\vec{R} - \vec{R_{e2}}; N_e - n\right)}{P\left(\vec{R_{e1}} - \vec{R_{e2}}; N_e\right)} \tag{2.4}$$

This expression represents the cumulative probability of finding any one of the monomers in the segment at a position in space such that the end points of the segment are separated by $\boldsymbol{R}$ and $\boldsymbol{R}_{e1}$ and $\boldsymbol{R}_{e2}$ are the distances between the position in space and each of the end points. N_e is the number of monomers in the segment. In the current study, we used the Gaussian form of the end to end probability in three dimensions.

$$P\left(\vec{R}; n\right) = \left(\frac{3}{2\pi n l^2}\right)^{3/2} exp\left(-\frac{3\vec{R}^2}{2nl^2}\right) \tag{2.5}$$

In this expression n is the number of statistical segments and l is the length of a statistical segment. The tabulated density clouds are generated from an integration of equation for the probability of finding any segment at a certain location in space, which represents the cylindrical symmetry of the density clouds. Density clouds were calculated and tabulated, so that the simulation could evaluate a density cloud through a less computational expensive linear interpolation, as was done by the original authors [33].

In the DCM framework, the entanglement network is a series of overlapping density clouds in addition to the network of entropy springs. To be physically consistent, the overlapping polymer density should evolve to the uniform bulk density of the simulated polymer, which is controlled by the equation of state for the probability density. Two affects make it desirable to modify the original equation of state for the density clouds. Firstly, the coarse-grained nature of the density clouds does not have enough detail to accurately resolve a realistic interface at the boundaries of the simulation. Secondly, it is desirable to have an energy landscape for the entanglement points such that a conjugate gradients relaxation method will find the global minimum in free energy for the entanglement network at each simulation step [33], something difficult with the original formulation. To accommodate these affects the equation of state was simplified to the equation below, a form that can be intuitively modified to achieve consistent results over several stretching cycles.

$$A_{total}/\rho = \begin{cases} 0 & \text{if } \rho < \rho_m \\ C\left((\rho-\rho_0)^2 - (\rho_m-\rho_0)^2\right) & \text{if } \rho \geq \rho_m \end{cases} \tag{2.6}$$

This expression was modified for constants ρ_m and C. The constant ρ_0 is chosen to be the bulk density of the polymer, because the minimum of the normalized free energy density is where the entanglement network relaxes to. The equation of state can be interpreted as a rule to force the entanglement points to adjust such that the polymer density is uniform throughout the simulation space. The final parameters were chosen so the system maintains the bulk polymer density and the conjugate gradient relaxation method produces consistent results over multiple stress cycles. Along with the simplification of the equation of state, we have assumed that fluctuations in the

density are constant throughout the simulations and the reported stress is not directly affected by the density cloud free energies.

The density cloud simulations use periodic boundary conditions in the uniaxial strain dimension. The lateral dimensions involve a free surface whose thermodynamics are governed by the density cloud equation of state. Periodic conditions in all simulation dimensions would be difficult with the density clouds as the numerical discretization used to integrate the density clouds needs to be relatively large (~10 Angstroms) and thus preserving volume is difficult as each dimension of the simulation cell must be an integer multiple of the density cloud discretization length. With the free surface in the lateral dimension the system can continuously adjust to preserve volume. Simulating an interface is also attractive for capturing effects such as the failure of an adhesive interface [33].

Two additional simplifications to the DCM are introduced for convenience. The first is that segment breakages are not allowed to occur. In this work, the full non-linear potential is used to represent the entropy spring terms of the free energy, and thus the rest positions of entanglement points always settle on positions where no chains are fully stretched, or over-stretched representing a non-physical condition. The second omission is that chains are allowed to cross one another without forming an additional entanglement point. The DCM authors chose to detect segment crossing and represent it by the addition of an entanglement point. The simulations reported here would differ with this consideration as a modest amount of chain crossings were observed; however, this study is limited to systems without loss of entanglement points due to slippage out, thus the number of entanglement points is constant.

Long time simulations are feasible due to the Kinetic Monte Carlo description of the entanglement dynamics and temporary bond breakage. Reptation dynamics are accounted for by allowing slippage at entanglement points, where polymer from one side of the entanglement point will transfer to the other side of the entanglement point which belongs to the same molecule. Instead of calculating particle trajectories, each simulation time step involves relaxing to an overall system minimum free energy. This is similar in spirit to traditional Monte Carlo, which has been used to calculate network stress [85-87], but in addition captures a sense of real time by defining rates of slippage and temporary bond breakage. The added benefit of simulating real dynamics is that failure of the polymer system may be captured more naturally compared to pure Monte Carlo methods.

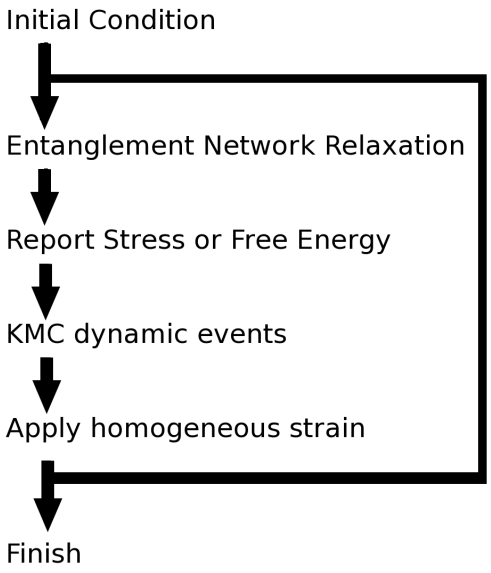

Figure 2: Schematic diagram of the simulation algorithm. This KMC/energy relaxation scheme handles the dynamics of the system through specified kinetic events and at each time step the system is relaxed to its global free energy minimum.

A simulation consists of repeating the following steps; relax the entanglement network to its free energy minimum, simulate Kinetic Monte Carlo events, and finally evolve the system the according amount of time from time dependent straining (Figure 2). It is important to note that although this method does handle dynamics, entanglement points do not have velocities or momentum at each time step, rather the free energy of that configuration is calculated through the entropy spring treatment of polymer segments.

The considered simulation events are described using Transition State Theory.

$$r = \nu e^{(U-\Delta A_{event})/k_B T} \tag{2.7}$$

For this equation r is the rate of the kinetic event. For the temporary bond kinetic event, υ is the thermal vibration frequency of the temporary bond taken to be 10^{12}, U is the activation energy for breaking the bond taken to be 20 kcal/mol, ΔA is the energy stored in the temporary bond, and the simulation temperature is 25C. These parameters are the same used in the studies by Termonia [4-8]. To simplify the comparison of the TBM and DCM the studies reported here are limited to systems without entanglement slippage. This simplification may more closely represent crosslinked networks with chain length equal to the molecular weight between entanglements; however, they will still be referred to as entanglement networks.

The overall stress of the simulation is calculated differently for the TBM and the

DCM. In the TBM conditions are not periodic and the stress is the sum of the strain dimension components of the forces of each of the elements involving the fixed entanglement points at the top or bottom of the simulation. The DCM stress must be calculated by taking the derivative of the free energy, which can be readily calculated at each step. The numerical method used for calculating this derivative was a five-point finite difference method.

2.3 Extension to 3D of Temporary Bond Model

The temporary bond model from literature was in 2D. A fully three-dimensional representation of the entanglement network is desired for comparison to the density cloud model, as well as for future inclusion of three dimensional microstructure. In the transition to three dimensions, Gaussian statistics for the segments between entanglement points should be maintained (i.e. initial stretched distance is that of a random coil $r = \sqrt{n}l$). In order to achieve this and also have a physically accurate polymer density, the simple "diamond" connectivity, named such for its equivalence to the carbon crystal structure for diamond, cannot be used.

The regular two-dimensional connectivity used in the original study [5-8] is only one of the possible configurations of connecting the entanglement points, and its ordered nature may not be physically realistic. Ways of producing entanglement networks from more detailed simulations have been conceived using the Primitive Path Algorithm (PPA) [50-51]. For this study a simpler method is used. The connectivity of the entanglement points are altered in a random fashion using a Reverse Monte Carlo algorithm, while preserving the polymer density until the segments between

entanglement points are acceptably close to their random coil configuration.

First a three-dimensional network of diamond connectivity is made such that the bulk density matches that of the polymer bulk density. In this configuration the stretched distance of the segments between entanglements is roughly half of the random coil configuration for MW_e equal to 14 statistical segments used for the temporary bond simulations (Figure 3). After this a reverse Monte Carlo algorithm is started that seeks a configuration where the segments are closely matched to the random coil configuration. The Monte Carlo move involved is a switching of one segment end point with that of another segment (Figure 4). The Metropolis algorithm is used with the artificial internal energy of the network below.

$$U_{randomcoil} = C \sum_{allsegments} \left(\frac{r}{nl} - \frac{r_{correct}}{nl} \right)^2 \tag{2.8}$$

In this equation C is a constant selected so that configuration space is sampled at a fast rate, r is the segment stretch distance, n is the number of statistical segments and l is the length of the statistical segment. When using this procedure to generate an initial condition for the density cloud model, a second iteration of the reverse Monte Carlo is needed after the initial configuration is simulated to find the zero strain condition. The zero strain condition may have some artificial segment alignment if the simulation length is different from the initial condition length, and a second iteration of connectivity alteration fixes this. The zero strain condition of the TBM is controlled by the temporary bonds and does not require the second iteration. The segment stretch histograms at various stages of this procedure is shown in Figure 2. The final relaxed condition for the density cloud simulation has an average somewhat less than the

random coil statistics after the RMC procedure, but the orientation of the segments remains uniform.

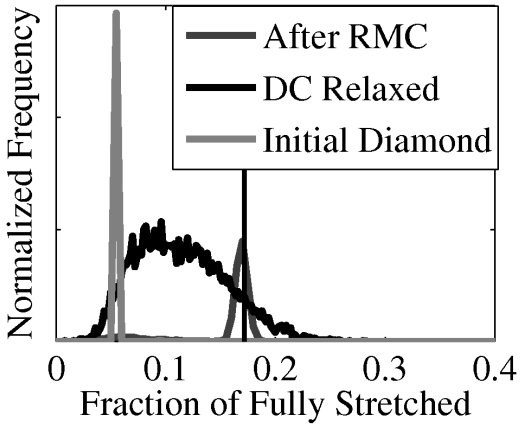

Figure 3: Segment stretch histograms for entanglement networks with: diamond connectivity; realistic connectivity from the Reverse Monte Carlo; relaxed zero strain condition after the second iteration. Vertical line is the value for random coil statistics for segments of 34 statistical units. The final average stretch of the Density Cloud simulations is between random coil statistics and diamond connectivity assumption.

When preparing systems involving polymer of a known molecular weight, a second reverse Monte Carlo treatment is used. In this instance, the internal connectivity of the entanglement points is important for keeping track of which direction each of the polymer chains involved in the entanglement point enter and exit the entanglement point. The Monte Carlo moves involved are; switching the internal connectivity of an entanglement point, and switching the marking a segment to be cut, which later will resulting in two chain ends (Figure 4). Both these moves alter the polydispersity of the entanglement network and the following equation for the internal energy is used to guide the system to monodispersity.

$$U_{molecularweight} = C \sum_{allchains} \left(\frac{MW}{MW_e} - \frac{MW_{correct}}{MW_e} \right)^2 \tag{2.9}$$

Using this treatment after the first reverse Monte Carlo treatment will result in an entanglement network with the desired molecular weight of polymer chains and the segments between entanglement points close to the random coil configuration. This method was used for the reported 3D TBM simulations. In contrast to the self-avoiding walk method used in the original TBM publication, this method does not concentrate chain ends around regions where a full length chain cannot fit into the entanglement network.

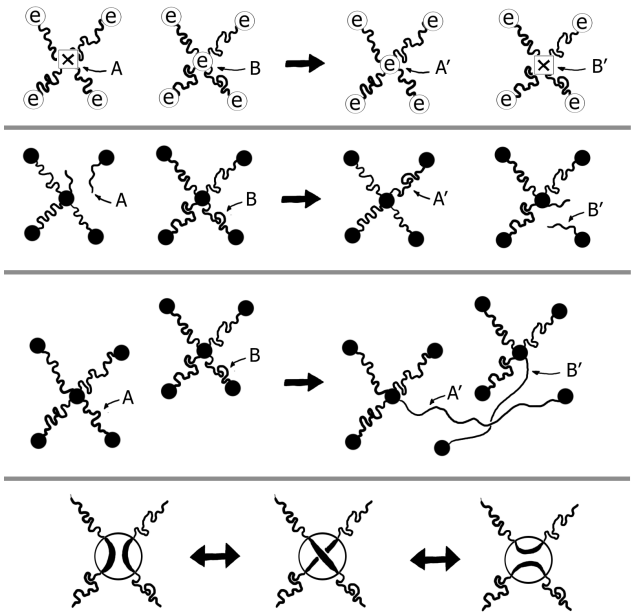

Figure 4: Schematic representation of the RMC moves (from top to bottom): entanglement point/crosslink point switch; chain end entanglement strand switch; segment neighbor switch; and internal connectivity change.

2.4 Temporary Bond Model Results

The authors of the temporary bond model [4-8] studied the model while varying many conditions including temperature, MW_e and MW. Here we are taking a single condition from their first publication as the system for extension to the three-dimensions. The system is polyethylene with molecular weight of 9500 and without slippage. A constant rate of elongation of 5 min^{-1} was used, whereas the authors use the same value for a constant rate of strain. All other simulation parameters are taken from the original publication [4], representing a mapping to molten polyethylene, including MW_e=14 statistical segments and density of 0.96 g/cm^3 or 4.13 statistical segments/l_{Khun}^3.

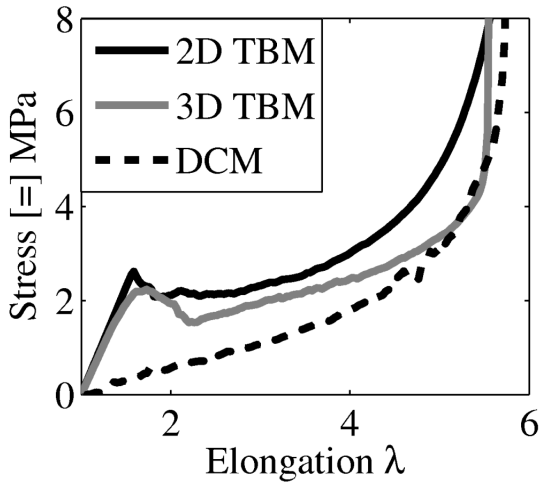

Figure 5: Comparison of the stress response of the 2D TBM with the 3D TBM with realistic connectivity and as density cloud simulation of an analogous system. Differences in the 2D and 3D TBM are strictly related to the changes in initial configuration due to the realistic connectivity.

As seen in Figure 5, the stress response is largely intact from the translation to three dimensions and using the Reverse Monte Carlo algorithm. The difference for the realistic connectivity is understandable considering starting conditions contain all possible starting orientations of segment vectors rather than the limited orientations from the diamond-connectivity network. For example, the upturn at high strain due to the finite extensibility is sharper due to shorter paths of elastically active chains bridging the neck of broken temporary bonds, accomplished by containing some oriented segments. All expected regions of the stress response are present, and thus their molecular interpretations remain unchanged from when originally published.

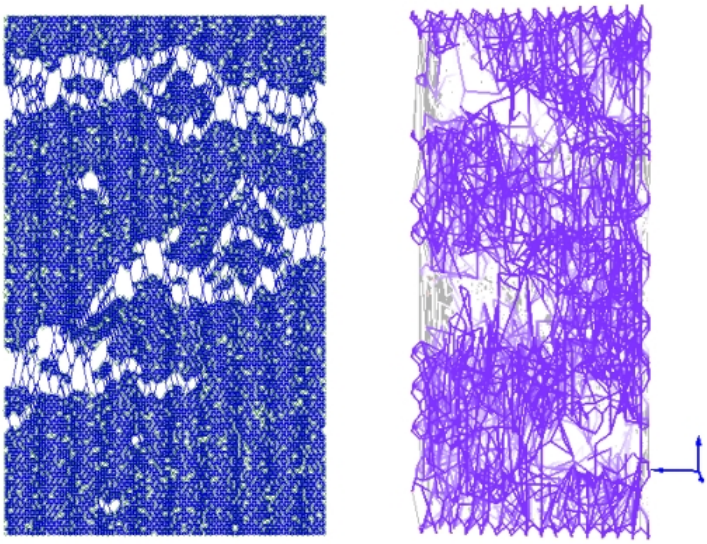

Figure 6: Visual representations of the 2D and 3D TBM highlighting the regions with existing temporary bonds to show consistencies between their morphological characteristics. Large regions of cooperatively broken temporary bonds represent necks which grow as the sample is stretched further.

An important success of the TBM is its ability to predict the evolution of morphology of the polymer sample [6]. The cooperative nature of the temporary bond breakage leads to heterogeneous regions of broken or still existing temporary bonds. The predicted morphologies of the two dimensional and three dimensional TBM are in good agreement with one another, as can be readily seen in Figure 6. These morphological characteristics are likely determined from the locations of the chain ends in the initial condition of the simulation. Temporary bonds over a segment representing a chain end are likely to break first, because they are not reinforced by the entropic spring of a polymer segment.

2.5 Density Cloud Model Results

The density cloud model involves discretizing space in order to numerically evaluate the free energy due to the overlapping density clouds. The value of the spatial discretization length was studied, and a value was found such that repetitive straining of a sample, without dynamic events, resulted in a consistent stress response between cycles. Achieving this also involved modifying the equation for the density cloud free energy such that interface effects on the lateral dimensions of the simulation would not dominate the relaxed positions of the nodes and the entropy spring contributions to entanglement point rest positions were balanced with the density cloud contribution. This involved a manual tuning of the minimum of the normalized free energy to a shallower profile, compared to the value used by the model authors. Our studies use ρ_0=0.90 g/mL or 4.54 statistical segments/l_{Khun}^3 to represent polypropylene, as the original density cloud authors used. ρ_m was set to 3.0 statistical segments/l_{Khun}^3 and C

was set to $0.003k_BT$. These values represent an alteration to the original density cloud free energy expression of roughly scaling down by two orders of magnitude. The value for spatial discretization that was $1*l_{Khun}$ or 12.0 Angstroms for the model system of polypropylene and N_e=34 uniformly throughout the density cloud simulation. For illustration purposes, visualizations of a relaxed system with discretization lengths of $1*l_{Khun}$ and $3*l_{Khun}$ is shown in Figure 7. For comparison to the TBM, the parameters of ρ_0=4.13 statistical segments/l_{Khun}^3, ρ_m=2.75 statistical segments/l_{Khun}^3, and C=0.01 k_BT were selected.

The discretization length of $1*l_{Khun}$ was selected as the maximum special discretization to accurately capture the density cloud behavior for the polypropylene system. This can be illustrated by observing the force an entanglement point feels with respect to it position in an entanglement network of diamond connectivity (Figure 8). It is important to ensure that the deviation from the finer results is not due to resolution of the density clouds and only to the discretization of the integration of the equation of state. To ensure this the $3*l_{Khun}$ discretization employed a nine point weighted averaging technique when calculating the contribution of a density cloud to a given volumetric unit. In the finer systems the contribution of a density cloud was calculated via the probability density at the center of each volumetric unit. Thus, the 1 and 3 l_{Khun} have the same density cloud resolution, while the discretization for free energy integration are different. Slight low amplitude periodicity in the force profile for $1*l_{Khun}$ spacing is due to entanglement point moving in and out of the sampling locations, and is small enough to be ignored. For the $3*l_{Khun}$ system without the nine point averaging technique, this periodic effect dominates the force profile. Additionally, using the original equation of state for the density clouds would result in

a roughly two orders of magnitude increase in the density cloud contribution for that shown in Figure 9. For the comparison to the TBM the discretization needed to be scaled down to $0.4*l_{Khun}$ to represent segments of 14 statistical segments as apposed to 34.

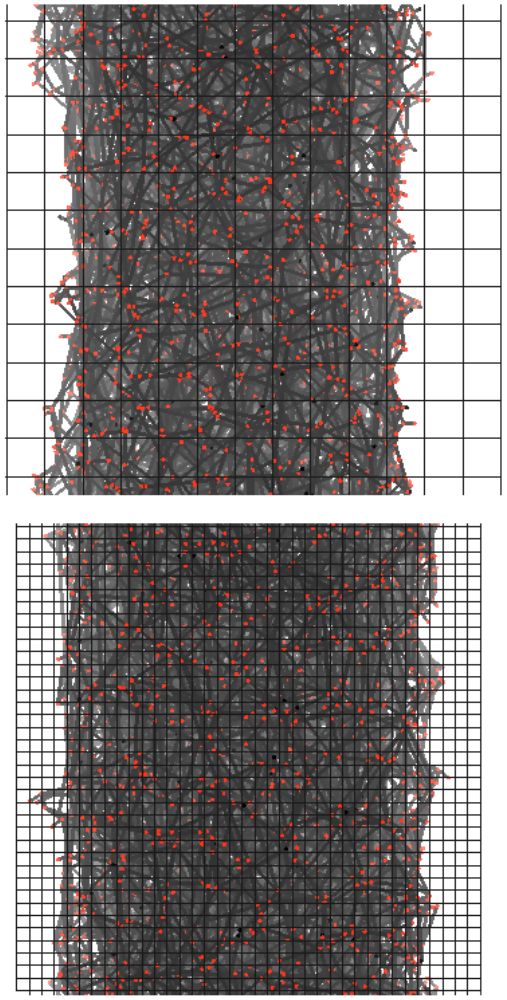

Figure 7: Orthographic projections of relaxed entanglement networks (34 statistical segments) with actual spatial discretization superimposed (spatial discretization lengths, top: $3.0*l_{Khun}$, bottom: $1.0*l_{Khun}$. Spatial discretization of $1.0*l_{Khun}$ was needed to produce consistent results over multiple stretching cycles.

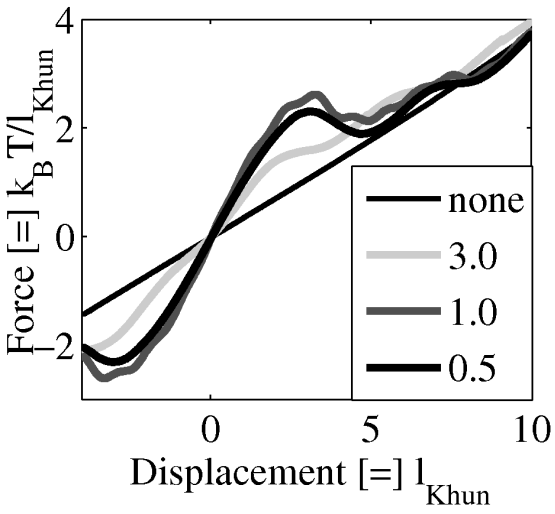

Figure 8: Local force profiles of a single entanglement point in a network of diamond connectivity. Three different spatial discretizations are shown, with the middle precision being the one selected for use (spacing=1.0*l_{Khun}).

Much can be said about the behavior of the density cloud from observation of their shape and individual entanglement point energy landscapes. The density clouds have the highest concentration of density at their fixed points of entanglement. The size of this peak decreases as the stretch of the polymer segment increases. In this manner the density clouds seem to adopt a configuration of entanglement point proximity such that no peaks are overlapping with one another. In the force profiles (Figure 8) the maximum associated with a high density cloud contribution is due to the entanglement point moving to a point of closest proximity to two neighboring entanglement points in the diamond connectivity entanglement network.

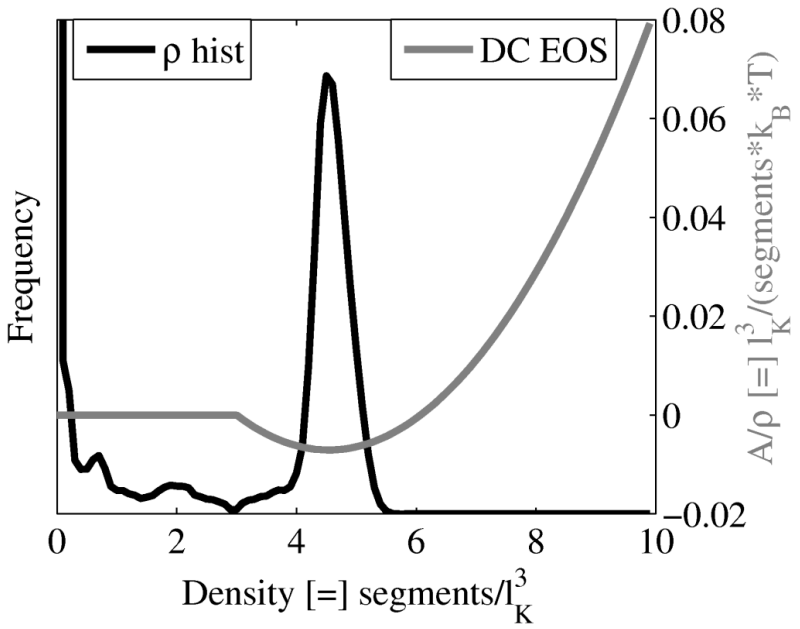

Figure 9: Histogram of the density of the volumetric discretized space superimposed on the modified equation of state for the overlapping density clouds.

As shown in Figure 9, the density clouds evolve the bulk density specified by the minimum in the normalized free energy expression for the density cloud equation of state. The average density, calculated by a weight average, stays virtually constant throughout the strain simulation. It varies by less than 5% over a strain range of 0 to 1.5, due to the growth of volume of the interfacial region.

In order to report the tensile stress of a sample, the simulation was allowed to undergo repetitive stress cycles from strains between -0.5 and 3.5 for five cycles. Typically after a small fraction of a single cycle the system settled into a stress response that was matched in subsequent cycles. Simulations using the original expression for the density cloud free energy exhibited hysteresis and a large amount of numerical noise suggestive of entanglement points being trapped in the non-global energy minimum

arrangements.

The density clouds serve to hold the entanglement network at its correct bulk density while allowing free relaxation of the entanglement points in all dimensions. The result of this is that the entanglement network stress ($1/A_0$*dA_{es}/dl) is close to that of the affine network theory (Figure 7), and not to that of semi-crystalline polymer. This suggests that the density clouds could serve as a framework of incorporated explicit crystallinity into an entanglement network to produce the semicrystalline response. In Figure 10, the density cloud result is compared to a result where all degrees of freedom of the entanglement points are fixed to their affine position and the lateral affine case. Each of these systems share the same starting point of the zero-strain density cloud entanglement network. Plotting the reduced stress of the affine network theory will produce a flat line and deviation from this in the affine simulation is due to the non-linear potential of the entropy springs. When modeled as linear springs the flat affine result is reproduced (not shown). The reduced stress of the density cloud simulation is of slightly lower value than the affine and lateral affine case because of the additional degrees of freedom to allow slightly non-affine deformation to occur.

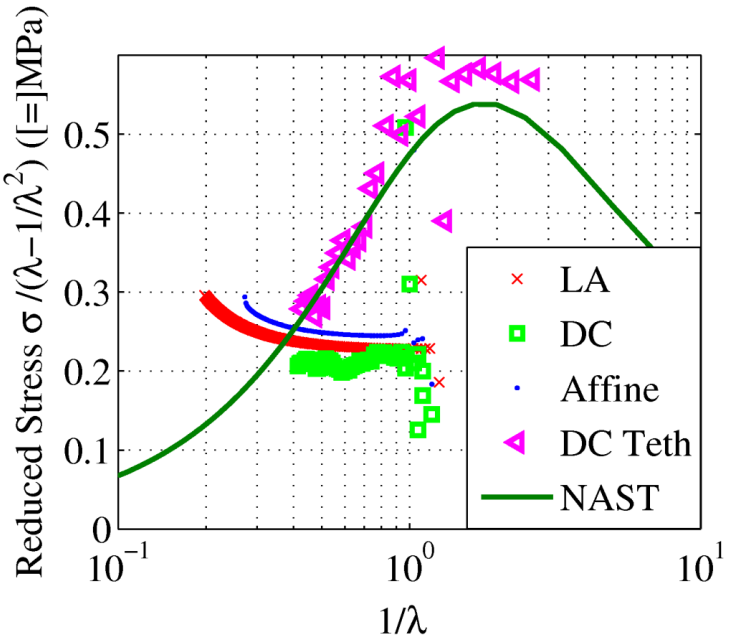

Figure 10: Reduced stress result for the density cloud simulation compared to the affine result and lateral affine result. Also shown is a density cloud simulation with non-affine tethering to and affine background and the fit to the Non-Affine Slip-Tube Theory.

Also shown in Figure 10 is a density cloud simulation with the addition of non-affine tethering to the affine background. Universal behavior of polymer networks have been shown to be modeled well by the Non-Affine Slip-Tube theory [60], and with that addition of the same non-affine tethering and entanglement slippage, behavior close to the universal behavior is captured. Carefully gauging the non-affine tethering, slippage and density cloud interactions is the topic of a later chapter. Non-affine tethering parameters are m_0=1, and the non-affine tethering are randomly displaced by an amount representative of the average random coil stretch distance of a 34 segment polymer. This random displacement leads to further stretching of the entanglement network strands and thus the higher reduced stress values.

The stress response of a system with 14 statistical segments between entanglement points and chain ends for the desired MW, analogous to that studied with the temporary bond model, is reported earlier in Figure 5. The chain ends in the density cloud simulation are modeled as an additional node for relaxation, but only affect one segment density cloud. The resulting stress calculated from the entropy spring contributions is suggestive of a polymer network response.

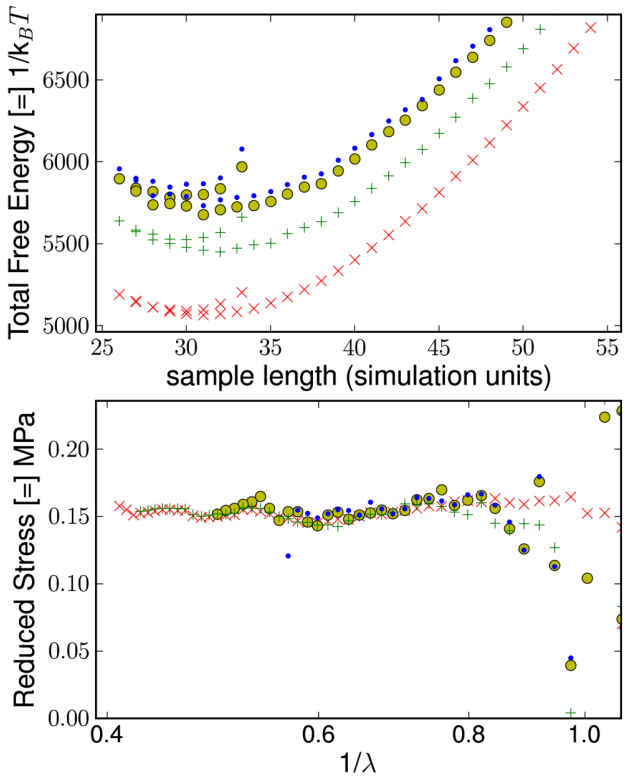

Figure 11: Free energy and reduced stress profiles for four density cloud simulations, with four different orders of magnitude for the equation of state constant *C*. The lowest in of the free energy profile is for the case with parameters reported in the text. The other three use each of the configurations from the base case and the energy relaxation is carried out again with the new equation of state with one order of magnitude greater value for *C*.

In order for the conjugate gradients relaxation scheme to find a global minimum at each simulation steps the simplified potential was introduced. The steepness of the normalized free energy curve at the minimum was roughly two orders of magnitude smaller than that of the function used by the original authors. This was a condition that led to reproducible stress response over several cycles; however, it is important to check that no other effects were lost in this large change. The density clouds have inherent behavior in common with non-affine network theories, which will be discussed in a later chapter, and it may be possible that certain types of interactions are affected differently by the simplified potential. To investigate this, the configurations at each step in the simulation was treated to another energy relaxation procedure with a different equation of state for the density clouds. Since these starting configuration are expected to be global minima, they should be a good starting point to see if any lost physics resurface. Using each configuration from the previously performed density cloud simulation assures that the artificial hysteresis from trapping in local energy minima does not occur. Figure 11 shows that no new physics are recovered from this process. The three orders of magnitude scaling factor of the simplified potential do have an affect of increasing the overall free energy of the system, the alteration is in such a fashion that the resulting stress, calculated from the derivative of the free energy, is unchanged. The larger free energy is a result of the packing of the density clouds being even more rigid with respect to the entropy spring terms that some additional local stretching occurs even though the overall density does not change.

Although a polymer chain made of several density clouds does have some

resemblance to a non-affine tube, the density clouds themselves still represent an ideal chain and are not generated in the presence of an external confining potential. One could speculate that: if the density clouds were generated with this in mind their shape would be different and may influence non-affine behavior.

2.6 Summary

The TBM was extended to three dimensions with characteristic stress response and morphologies of deformation intact. This involved introducing a RMC algorithm to generate a realistic initial condition for the entanglement network, and also allows for the direct comparison to the DCM.

By modifying the density cloud equation of state the DCM a consistent stress response from repetitive straining was recovered. This method has been shown to intrinsically handle excluded volume interactions of polymer segments between entanglement points, an improvement to the lateral affine assumption of the TBM. Furthermore, the DCM produces a soft rubbery stress response in contrast to the more rigid response from the original study of an adhesive interface. A study was conducted to confirm that a loss of some physics of the model was not a direct result of the modified density cloud equation of state.

The density cloud simulations involve an interface which was well behaved, but not characterized specifically. The level of coarse-graining makes constructing a first principles treatment of interfacial energies difficult; however, the density cloud equation of state may be tailored to a specific energy and this topic should be studied

further.

Elements may be added to a coarse-grained entanglement network to construct diverse behaviors, such as the temporary bond to recover a semi-crystalline stress response. Additionally, the level of coarse-graining of these models makes them promising to simulate long time and large length scale systems experiencing reptative dynamics. There are numerous complex systems that can be addressed in this framework, providing molecular level insight.

CHAPTER 3

HETEROGENEOUS MICROSTRUCTURE SIMULATION

3.1 Introduction

A key advantage to polymer simulation techniques is that they provide a straightforward way to introduce explicit phases into the system, and addressing complex systems is the motivation of many coarse-grained simulation techniques. In light of the DCM and lateral affine simulations producing a soft rubbery stress response (see Chapter 2), simulating a system with explicit rigid domains will serve as an additional system which will probe the behavior of the models in a new way.

A common method to achieve desired mechanical properties of polymer systems is combine different materials or other polymers with the system of interest. Polymer network nanocomposites are one such system that achieves desired mechanical improvements by the formation of clusters of rigid nanoparticles within a soft polymer matrix [125-126]. Such systems will be convenient for the desired coarse-grained simulation study because of the soft polymer matrix and cluster size scales feasible for entanglement network simulation.

One key application of nanocomposite polymer networks has been the addition of fillers, especially carbon black and silica, to rubber tires to enhance various properties, such as wet skid resistance, rolling resistance, and wear resistance [127]. Early studies in the 1960's were classified by Payne, who explained the non-linear viscoelastic behavior of carbon-black-filled rubber [128-130], by attributing the significant drop in

the storage modulus G' and the appearance of a maximum in the loss modulus G'' to the breaking and reforming of aggregates of filler particles.

With the growth of nanoscale fabrication techniques, polymer composite research has expanded and aims to achieve properties unattainable by conventional fillers [131]. Current research includes systems such as silica/PDMS nanocomposites [125-126], alumina/PMMA [132], and polyhedral oligomeric silsesquioxane (POSS)/PDMS [133]. Additionally, theoretical and simulation studies of nanocomposites have received much interest. These include theoretical studies of the hydrodynamic reinforcement [134], phase separation [135], and scattering patterns [136] of nanocomposite systems. Simulation studies using molecular dynamics [137-140] and Monte Carlo [131], have provided valuable insight to the development of model nanocomposites.

The following study aims to demonstrate the advantages of the DCM over an affine deformation assumption, and the nanocomposite topologies are not formulated from a first principles approach. The random formation of the network topologies bare similarities of the *in situ* formation of silica PDMS nanocomposites and reinforcement due to rigid domain loading will be studied.

3.2 Simulation Results

To test the models with a non-affine deformation, a spatially heterogeneous system was modeled. Such a system should highlight the ability of the DCM to allow for entanglement relaxation on all degrees of freedom, and to accurately account for

excluded volume interactions intrinsically through the individual simulation units.

To mimic in-situ generated silica nanocomposites, it is desired to generate entanglement networks with isolated rigid domains of tens of nanometers in diameter, representing small clusters of silica nanoparticles [125-126]. Under some conditions these domains will be chemically grafted to the surrounding network. To create such an entanglement network, rigid domains are superimposed on an entanglement network of zero strain from a Density Cloud simulation. To accomplish this, permanent bonds are added to segments which lie within the volume designated for a rigid domain. The centers of the rigid domains are not allowed to be within the diameter of the domains plus a small extra distance to ensure that no domains overlap. They are also required to be in the interior of the entanglement network.

For the reported experiments the diameter of the rigid domains is $10*l_{Khun}$ or roughly 10nm with an extra excluded distance of 0.2nm. Once an acceptable center is found for a rigid domain, all segments whose center point lies within the specified radius of the domain have a permanent bond activated, which behaves as a temporary bond but does not break. Activating these bonds does not ensure that all segments included in this domain are connected directly via permanent bonds. To correct this, additional segments with a permanent bond only are added as necessary to achieve a continuously connected rigid domain. The procedure for adding these additional bonds is as follows. If the next segment to be added to the rigid domain is not directly attached to any segment already in the rigid domain through an entanglement point, then a permanent bond is added between it and another segment already in the rigid domain. These added bonds will increase the modulus of these domains. The

modulus of these permanent bonds is set to a value such that the completely bonded entanglement network will produce an overall modulus of 1.6GPa, and with the additional bonds the modulus of the rigid domains will be larger than this by a small amount. This value for the permanent bonds was selected to be several orders of magnitude greater than the modulus of the underlying entanglement network, to ensure the domains are rigid.

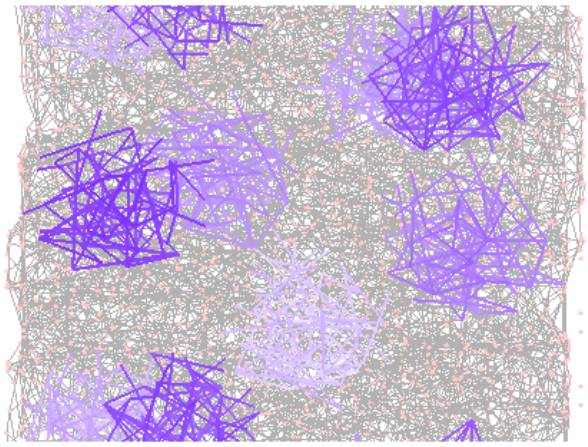

Figure 12: Visualization of a starting relaxed condition for an entanglement network with rigid domains of permanent bonds, with diameter 10nm. Temporary bonds are active in darkened segments. This sample dimensions are roughly 40nm per side and has 3500 entanglement points, the size used in all rigid domain simulations.

Formation of the rigid domains in this fashion does not alter the entanglement connectivity of the underlying network, and the domains are fully grafted to the soft matrix. A visualization of a starting entanglement network with rigid domains is shown in Figure 12.

This spatially non-homogeneous system was selected to highlight the advantages of having an intrinsic treatment of excluded volume, as in the DCM. The rigid domains should not deform throughout a strain experiment and all deformation will be concentrated in the entangled matrix and is no longer macroscopically affine in nature. Simulations using the lateral affine assumption will capture the rigid nature of the domains in the strain dimension but will not conserve the volume of the rigid domain. Additionally, domains will not have freedom to migrate laterally due to the lateral affine assumption, an effect that may be relevant at high particle loadings. The DCM framework handles these considerations intrinsically.

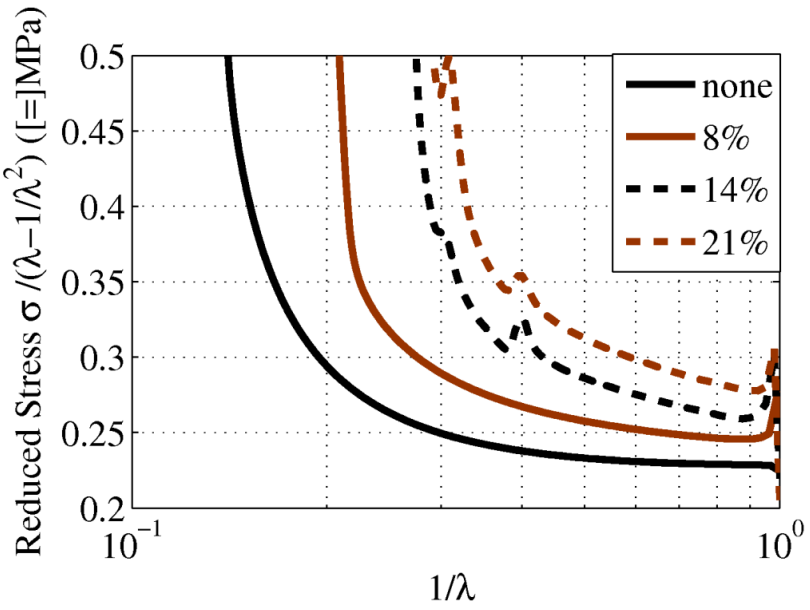

Figure 13: Reduced stress of rigid domain composites using the lateral affine assumption without density clouds. Results from entanglement networks without rigid domains and with four varying volume fractions of rigid domains are shown. High strain values can be easily achieved relative to the computationally expensive density cloud integration.

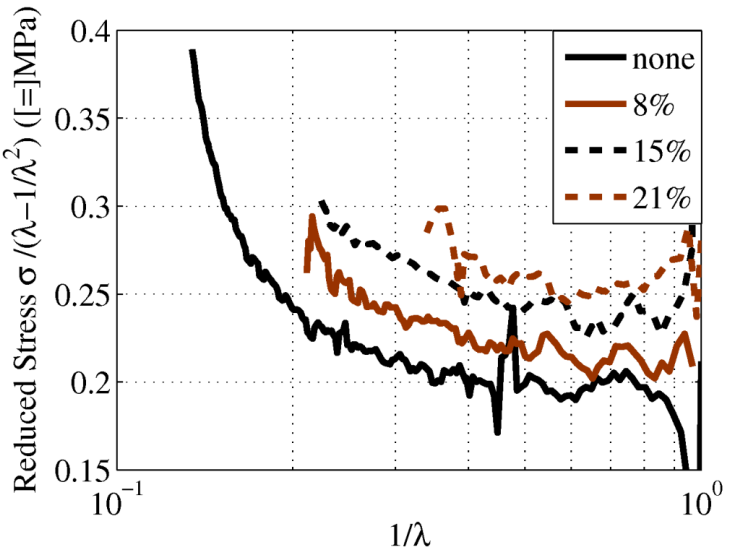

Figure 14: Reduced stress of rigid domain composites. The symbols represent simulations with density clouds for various rigid domain loadings. The lines represent data for 0%, 3% and 6% loading from the simulations without density clouds.

Lateral affine and DCM simulations are reported in Figures 13 and 14, respectively. For simplicity slippage and chain ends are not simulated to help isolate the comparison of the two models. In both cases the deformation is concentrated in the soft matrix as is evident by visualizing the simulations as well as by the reinforced modulus being of the order of magnitude of the non-reinforced system and not that of the rigid domain modulus.

In the case of no rigid domain placement, the system is behaving as a polymer network with molecular weight between crosslinks equal to the molecular weight between entanglements. This is because slippage is not modeled and the entanglement points are effectively crosslink points. This leads to a non-linear upturn at an earlier

strain than most experimental networks or nanocomposites.

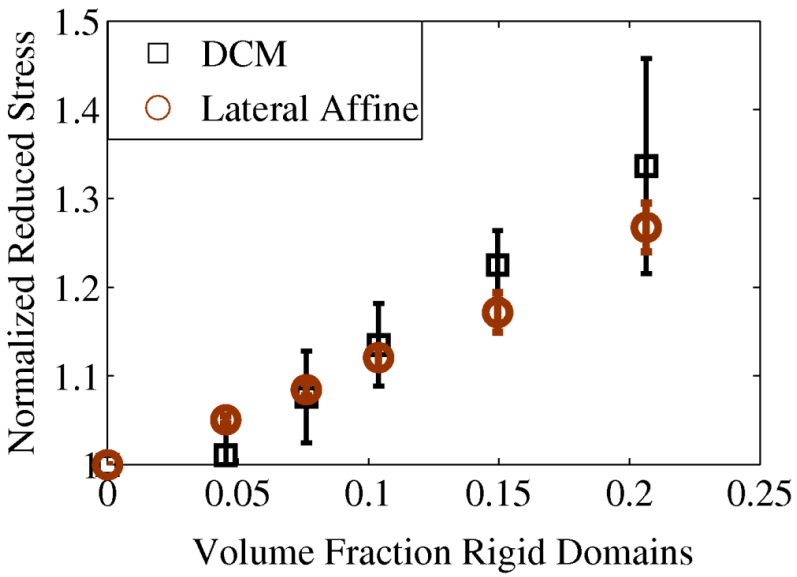

Figure 15: Effect of rigid domains on initial modulus in entanglement network simulations with and without density clouds. Plotted is the average reinforcement over a small range of low strain (~0.16-0.7). Both experience concentration of deformation in the soft matrix as the reduced stress is of the order of the soft matrix. The linear reinforcement from the density cloud simulations is suggestive of isolated particles.

The degree of reinforcement at low strain for the two models is summarized in Figure 15. The proportionality of the reinforcement and volume fraction of rigid domains suggests the rigid domains are behaving independently of one another. As noticed from the reduced stress curves, the DCM generally produces smaller stress values than the lateral affine assumption due to retaining all three dimensional degrees of freedom of the entanglement points. By comparing the relative reinforcements of the two methods the models predict the same trend of reinforcement. The trend suggests the

factor of reinforcement is equal to the fraction of rigid domains, i.e. a volume fraction of 20% rigid domains produces a 20% increase in modulus, an effect of isolated reinforcement of the rigid domains. At higher loadings or higher strains the rigid domains interact in a more complex way.

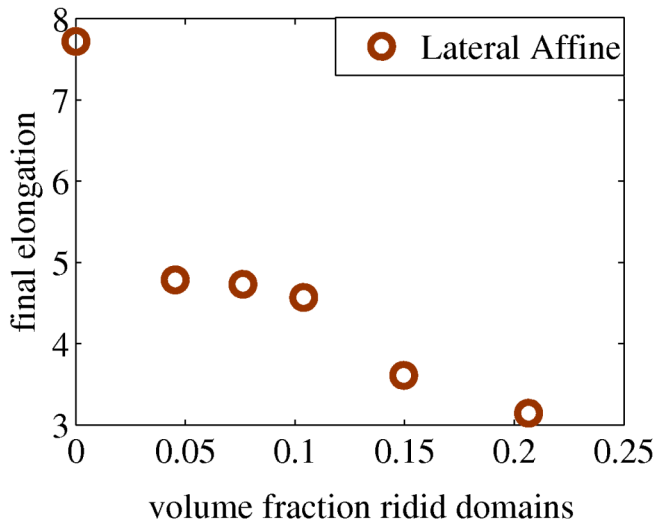

Figure 16: The elongation when reduced stress equals 0.45MPa, of the heterogeneous systems compared to the volume fraction of rigid domains.

The final strain from the lateral affine simulations is reported in Figure 16. The simulated stress turns upward rapidly near the final strain, as some chains approach fully stretched. The value of elongation is reported when the reduced stress reached 0.45MPa. At this value the all reduced stress plots have a very high slope and will be a good measure of when the entanglement network will ultimately fail. The final elongations for the systems with rigid domain loading of ~5%-10% are very similar due to a finite size effect. This is attributed to the same path of polymer segments becoming fully stretched leading to the stress upturn, as the higher domain loading

contain domains at the same positions of those in lower domain loadings. This could be addressed by much larger system size or an ensemble of rigid domain simulations with the use of considerable additional computation effort.

3.3 Summary

Entanglement network simulations of polymer network nanocomposites are achieved through the use of regions of permanent bonds of high force constant between entanglement points. Separate simulations involving the DCM or lateral affine assumption are used to report the reinforcement of mechanical properties based on the rigid domain loading of the nanocomposites. The rigid domains are shown to act independently at low strains before having multi-domain affects as is evident from the trend of final elongation to rigid domain loading.

The nanocomposite system highlights the intrinsic excluded volume interactions of the DCM, yet in extension, reinforcement effects are very similar between the DCM and lateral affine simulations. This study serves to demonstrate the potential of entanglement network models to simulate complex systems such as nanocomposites.

CHAPTER 4

POLYMER NETWORK SIMULATION

4.1 Introduction

Polymer networks have been a good system for developing theoretical ideas alongside experiments and simulations. In fact, many commonly accepted ideas in polymer physics, such as tube theories for polymers, were being developed with networks in mind.

The polymer network system is suitable to the entanglement network framework because of the elastic nature of the system, while being theoretically described by the tube picture of a polymer. The simulation protocol of energy minimization at each timestep fits well into an elastic polymer system, where momentum effects of the polymer units are ignored. Such is the case with the semi-crystalline systems of the TBM and DCM and here is applied to polymer networks. In this framework the dynamics of the system are described solely by the kinetics of slippage and/or temporary bond breakage, where applicable.

Furthermore, simulations of polymer networks analogous to the physical picture from network theories can lead to further insight into such models. This serves as the motivation to apply network theory ideas to the entanglement network framework.

Network theories are based on the idea of tethering a effective chain to a background that is deforming uniformly according to the macroscopic deformation of interest.

This allows the system to maintain its macroscopic shape without the explicit inclusion of excluded volume interactions. Secondly, the network theories are developed from the single chain picture and the network connectivity is accounted for through an end-to-end correlation function, thus forgoing an explicit representation of the connectivity of network strands.

These two fundamentals of network theories may be responsible for the lack of application of these theories to complex systems, such as nanocomposite networks, or bimodal networks. Likely, either of these ideas could be conceptually laid out in a straightforward manner, but may not have convenient mathematical representations.

A simulation analogue to these theories could handle the added complexity, as they would fundamentally rely on an explicit representation of connectivity of the network as apposed to ensemble average of effective chains. Similarly, the macroscopically deforming background can be abandoned to accommodate heterogeneous deformation which would be expected in heterogeneous systems.

4.2 Simulation Model

The TBM and DCM are already laid out in the tube-model representation of a polymer. In fact, the simulation unit of interest is the segment of polymer representing the molecular weight between entanglements. Polymer networks reported here are represented in a similar fashion with two slight modifications. Firstly, no chain ends will be represented as a perfect polymer network is a single molecule with no dangling ends. Secondly, some entanglement points will represent crosslinks, which will be

identical in their treatment except they will not be allowed to have slippage occur through them.

Keeping these considerations in mind, the previous method of entanglement network generation can be identically applied to the formation of the polymer network. The molecular weight altering RMC scheme can be slightly modified to allow for the specification of the crosslink strand molecular weight, as would be controlled in a physical network formed through an end-crosslinking reaction.

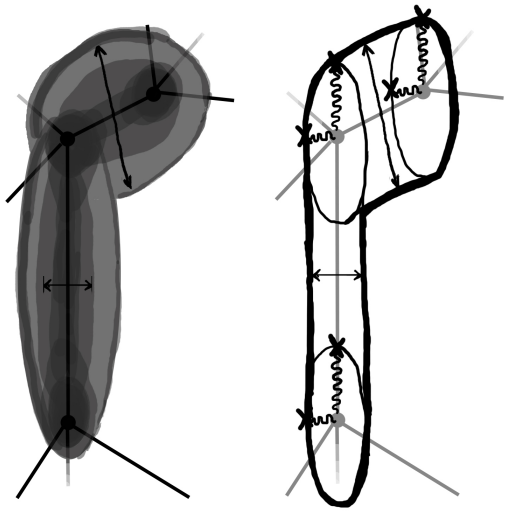

Figure 17: Schematic representation of the similarities of the DCM (left) and the NAT model (right). Two entanglement segments are shown for orientation along different axes where macroscopic deformation is extended along the vertical dimension. Notice the apparent similarities in the effect of orientation on tube diameter of the two models.

There are some apparent similarities in the model construction of the DCM and the Non-Affine Tube (NAT) model for polymer networks (Figure 17). The NAT model accounts for intersegment interactions by placing virtual chains regularly along the network polymer chain. The non-affine behavior of these tethering chains enters into the model solution by modifying the number of segments along the principle axes according to the macroscopic deformation, according to the following equation.

$$m_\alpha = \frac{1}{3} m_0 \lambda_\alpha^2 \tag{4.1}$$

where m_α is the number of segments of the virtual chain in a principle direction (α), m^0 is the starting number of segments, and λ_α is the elongation in the principle dimension. Figure 17 shows a rendition of the density clouds capturing a similar behavior to the tethering virtual chains. In both cases the axes of high deformation have extended segments and narrower confining tubes when compared to an axis of compression.

In addition to these possible similarities, the theoretical concepts themselves from polymer network theories can be added to a simulation. In fact, modifications to these proven concepts can be introduced without the worry of escaping a convenient mathematical form. Figure 18 illustrates this idea by comparing variations of the theoretical slip-tube from the Non-Affine Slip-Tube (NAST) theory [60] to slight variations used in this study.

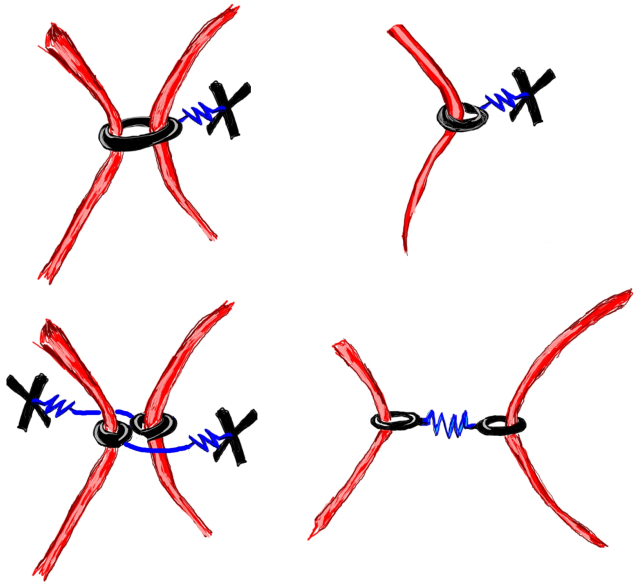

Figure 18: Conceptual representations of (counterclockwise from top right): entanglement from the NAST theory showing the slip ring attached to a virtual chain attached to the elastic background; virtual chain tethering added to a tetra-functional slip-link; decoupling of the tetra-functional slip link into two entanglement points each with a tethering virtual chain; the entanglement bond.

Since a tetra-functional slip-link is the fundamental unit of the entanglement network simulations, the most convenient way to introduce the non-affine behavior is by tethering the slip-ring to an affinely deforming background via a virtual chain. Additionally the entanglement points can be decoupled into two separate bi-functional entanglement points. This is technically the type of slip-link used in the NAST theory. A final representation in figure 18 is an entanglement bond. This concept is introduced as a way to introduce non-affine affects to the entanglement network without relying on a macroscopically deforming background.

4.3 Formation of Gaussian Entanglement Strands

Unique to the NAT and NAST theories is that the virtual chain tethers the entanglement points in such a way as to preserve the Gaussian nature of the segments between entanglements [60]. To accomplish this in the analogous simulations the following procedure is used. Starting from an entanglement network with specified molecular weight between crosslinks, all entanglement points are decoupled. The crosslinks maintain their positions in simulation space, but the entanglement points positions are disregarded and generated by simulating an ideal chain of entanglement points between the crosslinks. Firstly a zig-zag arrangement of the entanglement points is generated between the crosslinks such that the length of all segments between entanglement points is exactly the Gaussian average for the number of monomers it represents. It is believed that this is what the NAT author's meant from their explanation of the model. This is followed by random rotation moves of the entanglement points with respect to their neighbors, conserving the distances between the neighbors, a move typically used in Monte Carlo equilibration of chain systems. Enough of these moves are done for the system to represent a random flight of an ideal chain. The final step is to assign the virtual tether to each entanglement point in the exact location as to balance the forces of the two segments representing the polymer chain, and ensuring the initial condition is already at a free energy minimum with respect to the entropy springs.

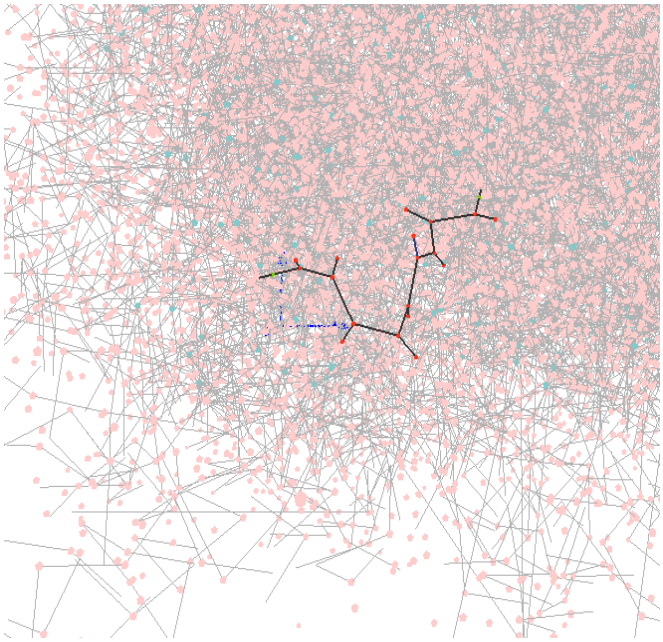

Figure 19: A single network strand highlighted in an initial configuration of an entanglement network representing a polymer network with Gaussian entanglement strands. In this diagram entanglement points and crosslink points are tethered to the elastic background. The virtual and real chains form a comb polymer, analogous to the effective strand of the NAT and NAST theories.

As seen in Figure 19, a large number of crosslink strands can be easily generated while conserving the network connectivity. In this fashion the simulation maintains the macroscopic shape of the polymer system rather than using an end-to-end correlation function from a single effective chain model.

Other initial conditions used in this study are slight variations to the one described above. A system generated by decoupling the entanglement points as above but keeping them at their initial locations, is used in the molecular weight study. Staying

at their initial location ensures that the starting condition of the entanglement network is uniform no matter which, or what fraction of entanglement points are converted to crosslinks. This is how networks of varying molecular weights between crosslinks can be generated and have very close to the same zero strain condition. Finally, in the study involving entanglement bonds, rather than completely decoupling the tetra-functional entanglements they are instead tethered to each other by an entanglement bond. The resulting rest position after this alteration will differ from before and the RMC condition before this treatment targets artificially stretched segments to compensate for the initial relaxation associated with the entanglement bond loading.

4.4 Effect of Slippage

The effect of slippage was not considered in the earlier study of comparison of the TBM and DCM; however, slippage was included in the original models, and its effect will be important here for reproducing realistic network behavior. Slippage accounts for the additional degrees of freedom when considering an entanglement point can move along either of the participating chains, or in the case of the NAST theories, the participating chain and the virtual tethering chain. Slippage in the TBM and DCM was modeled kinetically and was affected greatly by whether a yield point had been reached in the stress response. In the network theories, slippage is not a kinetic event but an additional degree of freedom leading to new configurations of the affective chain, all of which are considered in deriving the final stress. The simulations here are of the latter type, accomplished by giving the entanglement points an artificially high rate of slippage such that the minimum free energy configuration is achieved at each step with respect to entanglement slippage.

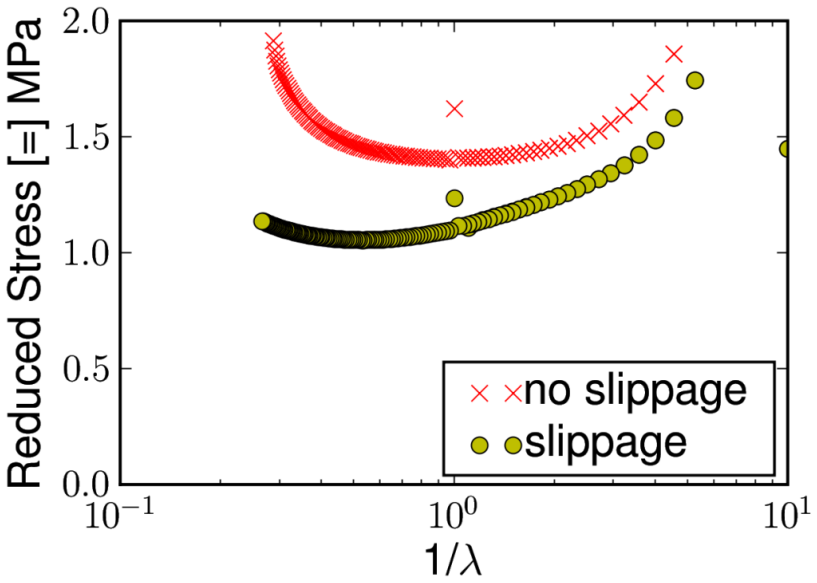

Figure 20: Reduced stress response of simulated polymer networks, with and without slippage. The networks represent an initial condition with crosslinks and entanglement points embedded in the elastic background throughout the simulation, to help highlight the affects of entanglement slippage. Upturns at high extension and compression are due to the fully non-linear representation of the entropy spring contributions of the polymer segments.

The affect of slippage is highlighted in Figure 20 where tetra-functional entanglement points are allowed to slip. The other degrees of freedom are removed and no excluded volume effects, density clouds or Lennard-Jones, are active. The system used the full non-linear representation of the entropy spring forces which leads to the stress upturn at high extension and compression. With the slippage events allowing to occur the upturns are delayed, by monomers from outstretched dimensions pass through entanglement points to segments that are more stretched. This effect under high extension is more pronounced because in this region the two non-strain principle

dimensions are under compression and are giving monomers to the segments oriented with the one dimension aligned with the strain. This interpretation is consistent with the network theories [60].

The system simulated in Figure 20 is has simulation parameters analogous to the system used for the DCM study, including N_e equal to 34 statistical segments and ρ_0 of 0.90 g/mL or 4.54 statistical segments/l_{Khun}^3.

It is important to note that there is a fundamental difference between considering all configurations as the network theories in contrast to just the minimum free energy configuration from this simulation methodology. The operating assumption is that the minimum energy configuration considered at each point in the simulation, which represents fixing entanglement and crosslinks in space, is such a degenerate configuration that is will dominate the statistics of all other configurations. This assumption seems reasonable as several monomer units are between each fixed point; however, some considerations of the theories will be restricted. For example, applying entanglement effect to each monomer is not possible in simulation, but possible with the NAT theory [141][60].

4.5 Molecular Weight Study Using Decoupled Tethering Entanglement Points

The network simulation will be fit the the functional form of the NAT and NAST theories and in doing so will have values for the crosslink and entanglement moduli, parameters G_c and G_e from the theories. These parameters serve as a direct measure of

independent contributions of the crosslinks and entanglement points respectively and observing these contributions independently is the goal of the molecular weight study. The molecular weight between crosslinks is directly correlated to the concentration of crosslinks. The concentration of crosslinks plus entanglement points is constant, by requiring a consistent bulk density and the molecular weight between entanglements is assumed to be independent of the crosslink molecular weight.

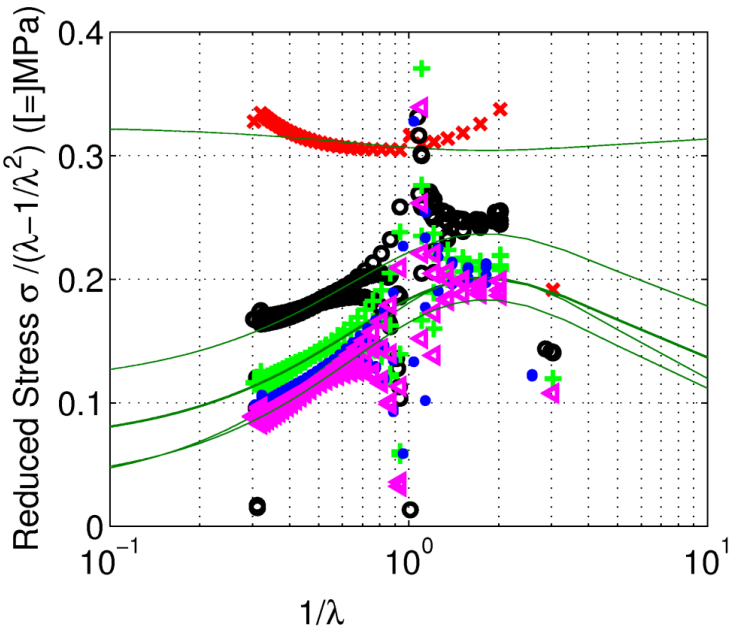

Figure 21: Simulations of polymer networks using decoupled entanglement points with non-affine tethering. Each curve represents a different crosslink strand molecular weight from MW_e to ~50 MW_e from top to bottom on the reduced stress plot. Each simulation is fit to the NAST theory and G_c and G_e are reported in the next figure.

Figure 21 shows a collection of simulations which vary only by which nodes are entanglement points and crosslinks, in accordance with the specified molecular weight of the crosslinks. The zero-strain condition is consistent between each molecular

weight sample as the decoupling and tethering of the entanglement points is done such that the entanglement points start at equilibrium. The parameter for the non-affine tethering chains are m_α the number of segments in the tethering virtual strand at zero strain is 10, and the number of segments change appropriately.

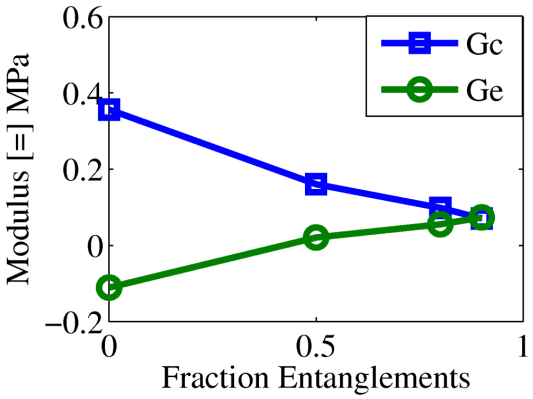

Figure 22: The crosslink and entanglement moduli plotted against the fraction of entanglements for the molecular weight study. In the framework of this study both moduli are directly proportional the concentration of the element they represent, crosslinks or entanglements.

The crosslinks in this study are not tethered to the affine background via virtual chains, but are rigidly embedded. This was chosen in contrast to the treatment in the NAT and NAST theories so that the system of entirely crosslinks would not have any non-affine effects, purely contributions from the crosslink modulus, G_c. This effect can be seen in Figure 21 and Figure 22. Under this simulation framework G_c and G_e are directly proportional to the concentration of the components that they represent. This relation provides a simple insight into how the molecular properties of the simulated networks influence the macroscopic stress response. This result serves as a

demonstration of the potential of such a technique and does not address the existence of diverse behavior for different networks, in terms of their relation of their bulk properties (MW_e and ρ) on the network moduli, G_c and G_e. Such a study would likely depend on the careful fitting of the tethering virtual chains as this will also have an impact on the reported G_e. A more careful analogue to the network theories will be addressed below.

4.6 Entanglement Bond Model

A main advantage to simulation is the ability to layer complexity in an explicitly into a model system. Many novel techniques exist to enhance polymer network mechanical properties, such as nanocomposites, or using model architectures such as bimodal networks. Such systems have not been addressed in theoretical models or with atomistic simulations, so the possibility of simulating them in a coarse-grained manor could be rewarding. This is the idea behind the entanglement bond formulation. Enhanced network properties will be dependent on adding inhomogeneities and thus the deformation can not be assumed to be macroscopically uniform. The entanglement bond formulation can bring the non-affine tube behavior of network theories into systems such as nanocomposites.

The entanglement bond will be different from the non-affine virtual tethering in some fundamental ways. Firstly, the entanglement bond should be isotropic so that they can freely rotate without introducing new stress. This is different from the non-affine virtual tethering which is anisotropic and assumes an affine deformation throughout

the sample space. Additionally, the entanglement bond should also be independent of the macroscopic strain. In light of these differences a potential for the entanglement bond can be fashioned in a consistent mean-field manor to capture some of the underlying physics of the non-affine tethering. The approach, proposed here, to evaluating this average is through an entanglement network simulation of tethered chains rather than evaluating an integral analytically.

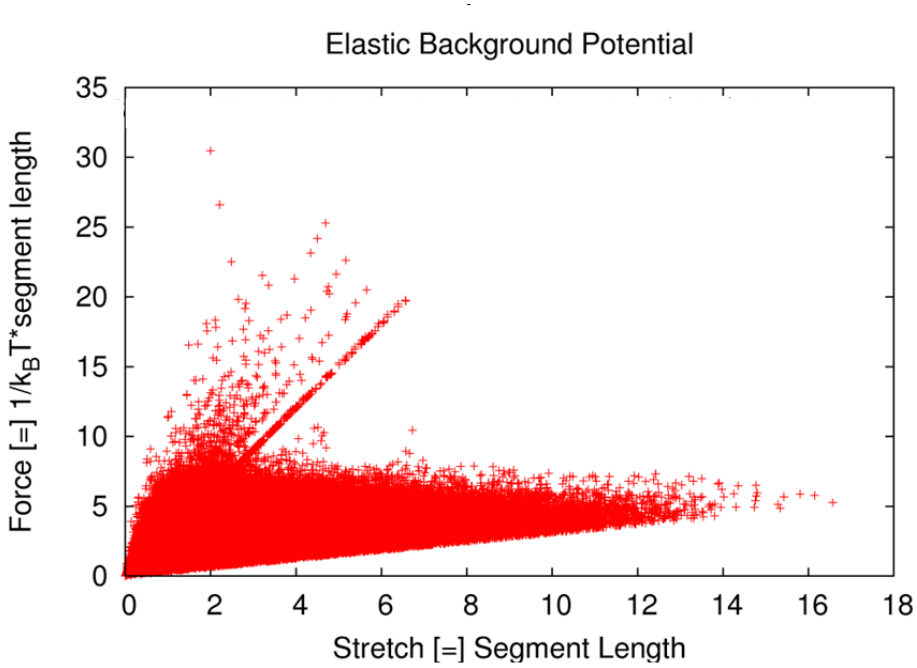

Figure 23: Plot of the force response of tethering virtual chains from a density cloud simulation with non-affine tethering. Plotted are the force response of the chains from all orientations, to represent the scatter of force profiles over which an ensemble average must be taken for a simple functional form of the entanglement bond.

Figure 23 shows the superposition of all virtual tethering potentials from all orientations and degrees of macroscopic deformations. Naturally a single expression

for all the virtual tethering chains will not be equivalent to the orientation and macroscopic strain dependent virtual tethering chains, but a potential representing the average of all the points above may go far to capture the behavior. The data seems to be consistent with the idea that as network chains become more stretched, the potential softens reducing the overall stress. This behavior was accounted for by explicitly modifying the tethering potentials based on the macroscopic strain, and could be handled by the entanglement bond through the network strands being of a lower stretch at zero-strain conditions, irrespective of orientation. Fitting a curve via least squares would be approximate to the ensemble average of all possible force profiles of a non-affine tethering simulation.

Figure 23 show an artifact from an early implementation of the network formation algorithm. The concentration of collinear data is due to identically oriented segments with the strain dimension on the edge of the initial conditions. This exists because of the non-periodic boundary conditions leave dangling ends of the "diamond" lattice formulation. This artifact was later resolved by pairing these dangling ends, resulting in completely tetra-functional nodal points, and is described in the Appendix.

Prior to performing the curve-fitting to the non-affine tethering behavior a functional form of softening potential was naively chosen.

$$\frac{F}{k_B T} = \frac{3}{2}\frac{log(r)}{nl^2} \tag{4.2}$$

This equation for the force of the entanglement bond was chosen to have the same stiffness at zero extension of the tethering virtual chains and share the expected

softening behavior through the incorporation of the logarithmic dependence on bond stretch, rather than linear of the Gaussian chain approximation.

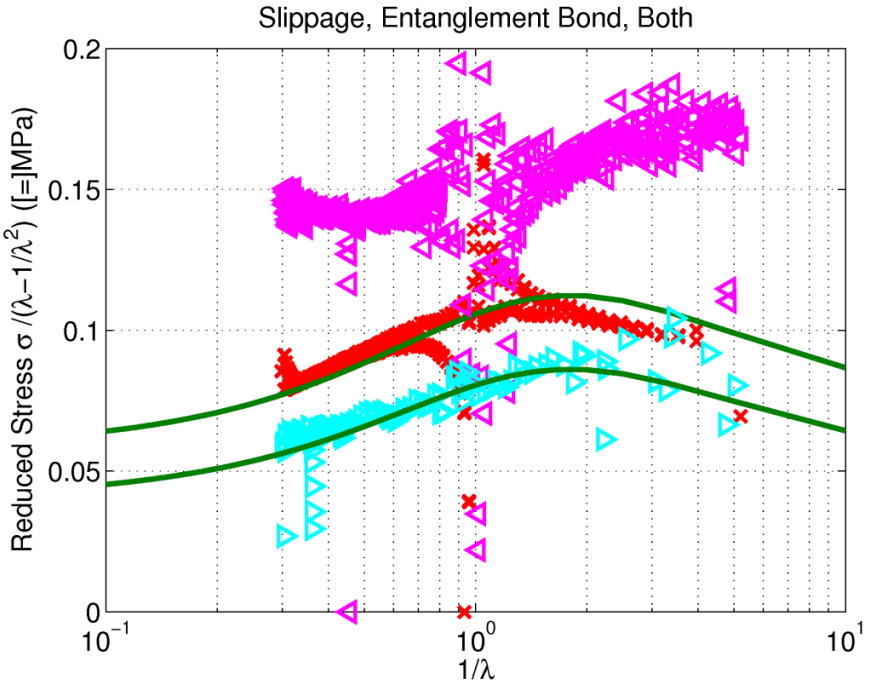

Figure 24: Plot of entanglement network simulations with periodic conditions in all dimensions to preserve volume. The three plots (from highest reduced stress to lowest) are with slippage activated but without entanglements converted to entanglement bonds; no slippage but entanglements converted to entanglement bonds; combination of slippage and entanglements converted to entanglement bonds. Entanglement bond function is logarithmic, and parameters from the density cloud study with 34 statistical segments between entanglements are used. Solid lines are least-squares fits to the Non-Affine Slip-Tube theory.

The logarithmic potential for the entanglement bond was used to simulate the behavior with and without slippage, and reported in Figure 24. Both slippage and entanglement

bond reduce stress from the affine network state, with a constant reduced modulus of ~0.2MPa. The affect of slippage on the reduced modulus has a characteristic of a uniform trend of higher modulus in towards compression. This is a reflection of uniaxial compression leading to the two, non-strain dimensions to have highly stretch chains whereas the remaining one dimension provides compressed chains to feed segments to the stretched chains. The converse is true in extension.

Alternatively, the entanglement bond effect results in a maximum in reduced stress at zero strain. This affect is attributed to zero strain being the configuration where the fewest segments are highly stretched. In compression or extension chains aligned with dimensions of extension pull on the entanglement bond function into the softening behavior of the logarithmic form resulting in a lowering of the reduced stress. Finally, in the case where both slippage is occurring and entanglements have been converted to entanglement bonds, a combination of the effects is scene and the shape of the curve resembles a balance of the two effects.

Figure 24 uses a least-squares curve fitting to NAST theory for the cases involving the entanglement bond. The universal behavior of the NAST theory is the ultimate goal of the entanglement bond formulation. NAST is a combination of slippage and non-affine tethering [60], just as the entanglement bond simulation with slippage combines these two affects. This provides a new interpretation of the NAST behavior as the best fit occurs when both slippage and entanglement bonds are present. This provides a possible insight into the Non-Affine Slip-Tube behavior by presenting the two effects decoupled from one another.

In light of this interpretation, a more refined simulation of both NAT and NAST theories was conducted to attempt to validate these observations.

4.7 Non-Affine Tube Model and Non-Affine Slip-Tube Model Simulation Analogues

To more closely match the NAT and NAST models, involves using the initial condition with decoupled entanglement points, with each entanglement point tethered to the affine background (Figure 18). Using the preparation procedure described above tetra-functional entanglement networks have their entanglement points decoupled and entanglement point positions randomly generated at the average Gaussian stretch distance.

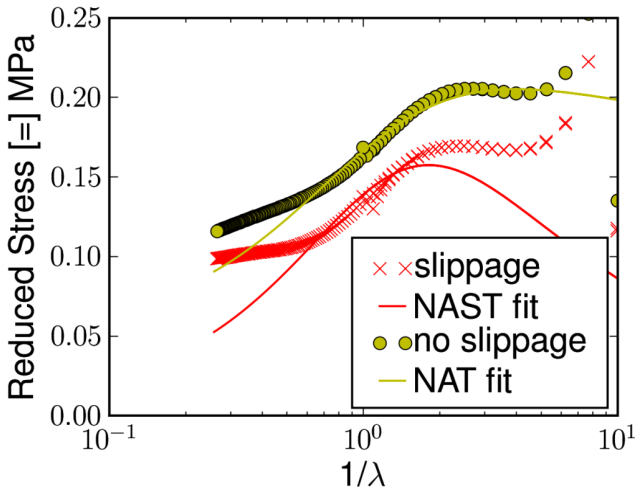

Figure 25: Simulation analogues of the Non-Affine Tube and Non-Affine Slip-Tube network models, and least-squares curve fits to the analytic expressions from the models. Simulations are using the parameters from the DCM study, including 34 statistical segments between entanglement points, and a crosslink strand molecular weight of 340 statistical segments with polydispersity near unity.

This network is simulated without slippage, as a close analogue to the NAT theory, and with slippage for the NAST theory. The results with their appropriate curve fits are shown in Figure 25. Some deviations between the simulations and network theories are observed, while sharing general behavior in common. The deviation of the network simulations at high strains are due to the increased strictness of the explicit network connectivity of the crosslink points. Simulations with crosslink points decoupled for each of the four participating network chains show a better agreement to the network theories which account for network connectivity through an end-to-end correlation function. Stress upturns at high compression are due to the non-linear entropy spring representation which the simulations use as apposed to the Gaussian chains of the network theory. This identical effect would appear at high extension if the simulations were allowed to continue.

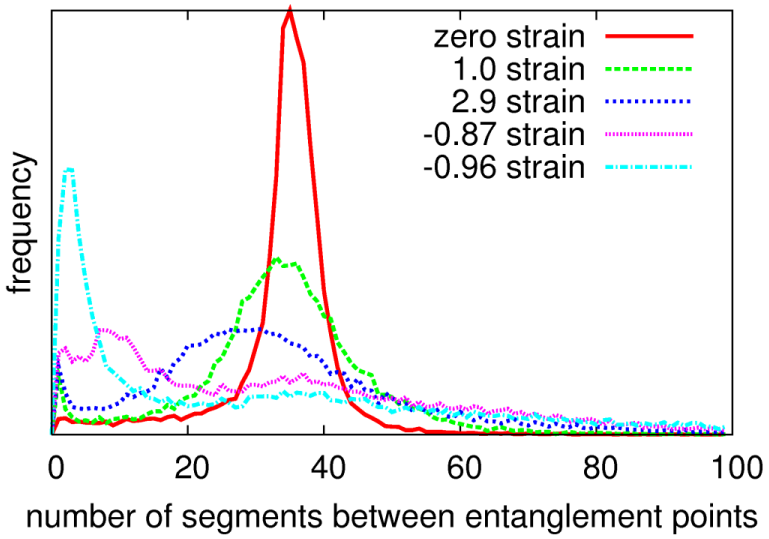

Figure 26: Evolution of histograms of number of segments between entanglement points for the non-affine network simulation with slippage. Shown are histograms from compression and extension compared to zero strain.

The affect of slippage does not have as a pronounced affect on the network simulations as in the network theories. Further investigation confirms that slippage is indeed occurring, as shown in Figure 26. Histograms of the number of segments between entanglement points change reproducibly from relatively monodisperse at low strain to having a broad shape and even concentration of segments with very few segments between entanglement points, at conditions of high compression and extension. This is consistent with slippage of non-stretched chains donating segments to chains of high extension.

Although the network picture with entanglement points space by the molecular weight between entanglements provides an intuitive representation of the network system, the NAT and NAST theories treat the entanglements at a much higher density [60]. To be consistent with the network theories the number of statistical segments of the tethering chains was fixed according to the following expression.

$$N_e \equiv 2\sqrt{pm_p} \tag{4.3}$$

Above, p is the number of segments between entanglement points in the network, and m_p is the number of segments of the tethering virtual chains and N_e is the entanglement molecular weight of the polymer. In the network theories an assumption of densely attached virtual chains is made ($p \ll N_e\lambda_\alpha$) which is not convenient from a simulation standpoint. Densely attaching tethering chains greatly reduces the number of configurations represented by the minimum free energy conformation with respect to all entanglement points, and brings into question the underlying assumption of the simulations that the single configuration with respect to the entanglement points greatly outweighs other configurations. Based on this difference, and the treatment of

explicit network connectivity in the network simulations, likely contribute to the differences observed in their representations of the network reduced stress.

4.8 Summary

Various methods of simulating polymer networks on the entanglement network scale have been conducted. Non-affine tethering affects have been incorporated from modern network theories. An entanglement bond element has been proposed and shown to capture the essential physics of NAST theory which is know to have a universal stress behavior of polymer networks. Additionally, analogues to the NAT and NAST theory have been simulated showing some agreement between simulation and theory. Differences between the theory and simulation are highlighted in light of some obvious discrepancies.

APPENDIX 1

A.1 Optimizing Density Cloud Integration

The entanglement relaxation algorithm involves evaluating the force of each entanglement due to the overlapping density clouds that participate in the entanglement point. Evaluating this is done using the following expression for all spacial unit cells (w index).

$$F_y = \frac{\partial A}{\partial y} = \sum \left[\frac{\partial \rho_w}{\partial y} \frac{\partial A}{\partial \rho_w} \right] \tag{A.1}$$

Since the derivative of the density clouds with respect to stretch and the polar coordinates from the centerline of the polymer segment are tabulated, the following expression is used by the simulation and involves a tabulated lookup for each of the three terms in the following equation.

$$\frac{\partial \rho_w}{\partial y} = \frac{\partial \rho_w}{\partial \alpha} \frac{\partial \alpha}{\partial y} + \frac{\partial \rho_w}{\partial x_s} \frac{\partial x_s}{\partial y} + \frac{\partial \rho_w}{\partial y_s} \frac{\partial y_s}{\partial y} \tag{A.2}$$

The optimizations employed in this study all focus on the reduction of number of tabulated lookup when considering the energy minimum location for a single entanglement point. The size of the simulation is such that a single entanglement point overlaps with a finite fraction of the overall simulation space. To reflect this, when the force expression is being evaluated, or when a density cloud is being subtracted and added back to the simulation due to an entanglement point move, each participating segment is considered independently. The boundaries of a single segments (of which entanglement points have four) overlapping density cloud is tabulated according to the stretch distance of the segments, and the integral is performed over the relevant area centered at the center point of the segment between entanglement points. This optimization allowed for the reported simulations to be

feasible with 2.4 GHz Pentium IV Dell workstations.

A.2 Parallelizing Density Cloud Integration

Further optimization was achieved through the parallelization of the density cloud integration. In cooperation with the optimization above, the integration for each segment between entanglement points was split between the two processors of the workstation to half the simulation time. This was accomplished using an OpenMP parallel "for" loop.

A.3 Generating Initial Diamond Connectivity with Periodic Conditions in One Dimension

To study the DCM it is desired to have a system with periodic conditions in the straining dimension only. The starting place of the RMC algorithm is the diamond connectivity which includes tetrafunctional nodes, but by imposing a surface in the lateral dimensions leads to dangling segments. To avoid this affecting the molecular weight RMC algorithm these dangling ends are pair with one another in the layers directly above or below, through the periodic strain dimension. This leads to a starting condition with the segments generated from dangling ends of a higher stretch than the other segments, which was always immediately followed by the RMC algorithm to achieve random coil statistics for the segments.

REFERENCE

1: Termonia, Y., Molecular Modeling Of Spider Silk Elasticity, *Macromolecules* ***1994***, 27, 7378-7381

2: O'Brien, J. P.; Fahnestock, S. R.; Termonia, Y.; Gardner, K. C. H., Nylons from nature: Synthetic analogs to spider silk, *Advanced Materials* ***1998***, 10, 1185-+

3: Rodriguez, F; Cohen, C; Ober, C. K.; Archer, L. A., ***Principles of Polymer Systems***, 2003

4: Termonia, Y.; Smith, P., Kinetic-Model For Tensile Deformation Of Polymers . 1. Effect Of Molecular-Weight, *Macromolecules* ***1987***, 20, 835-838

5: Postema, A. R.; Smith, P., Kinetic Model for Tensile Deformation of Polymers. 3. Effects of Deformation Rate and Temperature, *Macromolecules* ***1988***, 21, 3485-3489

6: Termonia, Y.; Smith, P., Kinetic Model for the Tensile Deformation of Polymers. 2. Effect of Entanglement Spacing, *Macromolecules* ***1988***, 21, 2184-2189

7: Termonia, Y.; Smith, P., Kinetic model for tensile deformation of polymers. Part IV: Effect of polydispersity, *Colloid and Polymer Science* ***1992***, 270, 1085-1090

8: Termonia, Y.; Smith, P., Kinetic Model for Tensile Deformation of Polymers. 5. Effect of Temperature on Orientation Efficiency, *Macromolecules* ***1993***, 26, 3738-3741

9: Mackley, M. R.; Solbai, S., Die-Free Spinning - A Method For Producing High-Performance Polyethylene Fibers And Tapes, *Polymer* ***1987***, 28, 1111-1114

10: Graessley, W. W., Viscosity of Entangling Polydisperse Polymers, *The Journal of Chemical Physics* ***1967***, 47, 1942-1953

11: Mark, J. E., The Use Of Model Polymer Networks To Elucidate Molecular Aspects Of Rubberlike Elasticity, *Advances In Polymer Science* ***1982***, 44, 1-26

12: Irvine, P. A.; Smith, P., Development Of The Axial Young Modulus With Draw Ratio Of Flexible-Chain Polymers, *Macromolecules* ***1986***, 19, 240-242

13: Postema, A. R.; Smith, P., Stiffness Of Oriented Flexible-Chain Polymers, *Macromolecules* ***1990***, 23, 3296-3301

14: Capaccio, G.; Crompton, T. A.; Ward, I. M., Drawing Behavior Of Linear Polyethylene .2. Effect Of Draw Temperature And Molecular-Weight On Draw Ratio And Modulus, *Journal Of Polymer Science Part B-Polymer Physics* ***1980***, 18, 301-309

15: Smith, P.; Lemstra, P. J., Ultra-high strength polyethylene filaments by solution spinning/drawing. 3. Influence of drawing temperature, *Polymer* ***1980***, 21, 1341-1343

16: Termonia, Y., Tensile strength of discontinuous fibre-reinforced composites, *Journal of Materials Science* ***1990***, 25, 4644-4653

17: Termonia, Y., Fibre coating as a means to compensate for poor adhesion in fibre-reinforced materials, *Journal of Materials Science* ***1990***, 25, 103-106

18: Termonia, Y., Structure-propery relationships in nanocomposites, *Polymer* ***2007***, 48, 6948-6954

19: Termonia, Y., Computer model for the elastic properties of short fibre and particulate filled polymers, *Journal of Materials Science* ***1987***, 22, 17733-1736

20: Termonia, Y., Theoretical study of the stress transfer in single fibre composites, *Journal of Materials Science* ***1987***, 22, 504-508

21: Termonia, Y., Molecular Model for the Mechanical Properties of Elastomers.1. Network Formation and the Role of Entanglements, *Macromolecules* ***1989***, 22, 3633-3638

22: Termonia, Y., Melecular Model for the Mechanical Properties of Elastomers. 2. Synergic Effects in Bimodal Cross-Linked Networks, *Macromolecules* ***1990***, 23, 1481-1483

23: Bicerano, J.; Grant, N. K.; Seitz, J. T.; Pant, K., Microstructural Model for Prediction of Stress-Strain Curves of Amorphous and Semicrystalline Elastomers, *Journal of Polymer Science Part B-Polymer Physics* ***1997***, 35, 2715-2739

24: Mansfield, M. L., Concentrated, Semiflexible Lattice Chain Systems and Criticism of the Scanning Technique, *Macromolecules* ***1994***, 27, 4699-4704

25: Reddy, B. K.; Estevez, R.; Basu, S., Revisiting the mesoscopic Termonia and Smith model for deformation of polymers, *Modelling and Simulation in Materials Science and Engineering* ***2008***, 16, 025008 (20pp)

26: Olaj, O. F.; Lantschbauer, W., Simulation Of Chain Arrangement In Bulk Polymer .1. Chain Dimensions And Distribution Of The End-To-End Distance, *Makromolekulare Chemie-Rapid Communications* ***1982***, 3, 847-858

27: Mansfield, M. L., Monte Carlo studies of polymer chain dimensions in the melt, *The Journal of Chemical Physics* ***1982***, 77, 1554-1559

28: Madden, W. G., Monte Carlo studies of the melt-vacuum interface of a lattice polymer, *The Journal of Chemical Physics* ***1987***, 87, 1405-1422

29: Madden, W. G., Numerical tests of a pseudoreactive algorithm for lattice chains, *The Journal of Chemical Physics* ***1988***, 88, 3934-3943

30: Madden, W. G.; Pesci, A. I.; Freed, K. F., Phase equilibria of lattice polymer and solvent: tests of theories against simulations, *Macromolecules* ***1990***, 23, 1181-1191

31: Terzis, A. F.; Theodorou, D. N.; Stroeks, A., Entanglement network of the polypropylene/polyamide interface. 1. Self-consistent field model, *Macromolecules* ***2000***, 33, 1385-1396

32: Terzis, A. F.; Theodorou, D. N.; Stroeks, A., Entanglement network of the polypropylene/polyamide interface. 2. Network generation, *Macromolecules* ***2000***, 33, 1397-1410

33: Terzis, A. F.; Theodorou, D. N.; Stroeks, A., Entanglement network of the polypropylene/polyamide interface. 3. Deformation to fracture, *Macromolecules* ***2002***, 35, 508-521

34: Creton, C; Kramer, E. J.; Hui, C. Y.; Brown, H. R., Failure Mechanisms of polymer interfaces reinforced with block copolymers, *Macromolecules* ***1992***, 25, 3075-3088

35: Washiyama, J.; Creton, C.; Kramer, E. J., TEM fracture studies of polymer interfaces, *Macromolecules* ***1992***, 25, 4751-4758

36: Washiyama, J.; Kramer, E. J.; Creton, C. F.; Hui, C. Y., Chain pullout fracture of polymer interfaces, *Macromolecules* ***1994***, 27, 2019-2024

37: Cho, K. W.; Li, F. K., Reinforcement of amorphous and semicrystalline polymer interfaces via in-situ reactive compatibilization, *Macromolecules* ***1998***, 31, 7495-7505

38: Boucher, E.; Folkers, J. P.; Hervet, H.; Leger, L.; Creton, C., Effects of the formation of copolymer on the interfacial adhesion between semicrystalline polymers, *Macromolecules* ***1996***, 29, 774-782

39: Boucher, E.; Folkers, J. P.; Creton, C.; Hervet, H.; Leger, L., Enhanced adhesion between polypropylene and polyamide-6: Role of interfacial nucleation of the beta-crystalline form of polypropylene, *Macromolecules* ***1997***, 30, 2102-2109

40: Scheutjens, J. M. H. M.; Fleer, G. J., Statistical-theory of the adsorption of interaction chain molecules .1. partition-function, segment density distribution, and adsorption-isotherms, *Journal of Physical Chemistry* ***1979***, 83, 1619-1635

41: Scheutjens, J. M. H. M.; Fleer, G. J., Statistical-theory of the adsorption of interacting chain molecules .2. train, loop, and tail size distribution, *Journal of Physical Chemistry* ***1980***, 84, 178-190

42: Scheutjens, J. M. H. M.; Fleer, G. J., Interaction between 2 adsorbed polymer layers, *Macromolecules* ***1985***, 18, 1882-1900

43: Fleer, G. J.; Cohen Stuart, M. A.; Scheutjens, J. M. H. M.; Cosgrove, T.; Vincent, ***Polymers at Interfaces***, 1993

44: Theodorou, D. N., Sturcture and thermodynamics of bulk homopolymer solid interfaces - a site lattice model approach, *Macromolecules* ***1988***, 21, 1400-1410

45: Fischel, L. B.; Theodorou, D. N., Self-Consistent-Field Model Of The Polymer Diblock Copolymer Polymer Interface, *Journal Of The Chemical Society-Faraday Transactions* ***1995***, 91, 2381-2402

46: Fischel, L. B.; Newman, J.; Theodorou, D. N., Segment density of a block copolymer chain tethered at both ends, *J. Chem. Soc., Faraday Trans.* ***1997***, 93, 4355-4370

47: Wijmans, C. M.; Leermakers, F. A. M.; Fleer, G. J., Chian stiffness and bond correlations in polymer brushes, *Journal of Chemical Physics* ***1994***, 101, 8214-8223

48: Wasserman, S. H.; Graessley, W. W., Prediction of linear viscoelastic response for entangled polyolefin melts from molecular weight distribution, *Polymer Engineering and Science* ***1996***, 36, 852-861

49: Fetters, L. J.; Lohse, D. J.; Richter, D.; Witten, T. A.; Zirkel, A., Connection between Polymer Molecular Weight, Density, Chain Dimensions, and Melt Viscoelastic Properties, *Macromolecules* ***1994***, 27, 4639-4647

50: Sukumaran, S. K.; Grest, G. S.; Kremer, K.; Everaers, R., Identifying the primitive path mesh in entangled polymer liquids, *Journal of Polymer Science Part B: Polymer Physics* ***2005***, 43, 917-933

51: Uchida N.; Grest, G. S.; Everaers, R., Viscoelasticity and primitive path analysis of entangled polymer liquids: From F-actin to polyethylene, *The Journal of Chemical Physics* ***2008***, 128, 044902

52: Tzoumanekas, C. and Theodorou, D. N., Topological analysis of linear polymer melts: A statistical approach, *Macromolecules* ***2006***, 39, 4592-4604

53: Tzoumanekas, C. and Theodorou, D. N., From atomistic simulations to slip-link models of entangled polymer melts: Hierarchical strategies for the prediction of rheological properties, *Current Opinion In Solid State & Materials Science* ***2006***, 10, 61-72

54: Werner, A.; Schmid, F.; Binder, K.; Muller, M., Diblock copolymers at a homopolymer-homopolymer interface: A Monte Carlo simulation, *Macromolecules* ***1996***, 29, 8241-8248

55: Muller, M.; Schick, M., Bulk and interfacial thermodynamics of a symmetric, ternary homopolymer-copolymer mixture: A Monte Carlo study, *Journal of Chemical Physics* ***1996***, 105, 8885-8901

56: Van Krevelen, D. W., ***Properties of Polymers***, 1997

57: Mark, J. E., ***Properties of Polymers Handbook***, 1996

58: Dowling, N. E., ***Mechanical Behavior of Materials***, 1999

59: Bicerano, J., ***Prediction of Polymer Properties***, 1993

60: Rubinstein, M.; Panyukov, S., Elasticity of Polymer Networks, *Macromolecules* ***2002***, 35, 6670-6686

61: Wall, F. T.; Flory, P. J., Statistical Thermodynamics of Rubber Elasticity, *The Journal of Chemical Physics* ***1951***, 19, 1435-1439

62: Flory, P. J., Statistical Thermodynamics Of Random Networks, *Proceedings Of The Royal Society Of London Series A-Mathematical Physical And Engineering Sciences* ***1976***, 351, 351-380

63: Mooney, M., The Thermodynamics of a Strained Elastomer. I. General Analysis, *Journal of Applied Physics* ***1948***, 19, 434-444

64: Rivlin, R. S., Large Elastic Deformations of Isotropic Materials. IV. Further Developments of the General Theory, *Philosophical Transactions of the Royal Society of London. Series A, Mathematical and Physical Sciences* ***1948***, 241, 379-397

65: Rivlin, R. S.; Saunders, D. W., Large Elastic Deformations of Isotropic Materials. VII. Experiments on the Deformation of Rubber, *Philosophical Transactions of the Royal Society of London. Series A, Mathematical and Physical Sciences* ***1951***, 243, 251-288

66: James, H. M.; Guth, E., Theory of the Elastic Properties of Rubber, *The Journal of Chemical Physics* ***1943***, 11, 455-481

67: James, H. M., Statistical Properties of Networks of Flexible Chains, *The Journal of Chemical Physics* ***1947***, 15, 651-668

68: Higgs, P. G.; Ball, R. C., Polydisperse Polymer Networks - Elasticity, Orientational Properties, And Small-Angle Neutron-Scattering, *Journal De Physique* ***1988***, 49, 1785-1811

69: Erman, B.; Flory, P. J., Theory of elasticity of polymer networks. II. The effect of geometric constraints on junctions, *The Journal of Chemical Physics* ***1978***, 68, 5363-5369

70: Flory, P. J.; Erman, B., Theory of elasticity of polymer networks. 3, *Macromolecules* ***1982***, 15, 800-806

71: Erman, B.; Flory, P. J., Relationships between stress, strain, and molecular constitution of polymer networks. Comparison of theory with experiments, *Macromolecules* ***1982***, 15, 806-811

72: Erman, B.; Monnerie, L., Theory of elasticity of amorphous networks: effect of constraints along chains, *Macromolecules* ***1989***, 22, 3342-3348

73: Kloczkowski, A.; Mark, J. E.; Erman, B., A Diffused-Constraint Theory for the Elasticity of Amorphous Polymer Networks. 1. Fundamentals and Stress-Strain Isotherms in Elongation, *Macromolecules* ***1995***, 28, 5089-5096

74: Edwards, S. F., Statistical Mechanics Of Polymerized Material, *Proceedings Of The Physical Society Of London* ***1967***, 92, 9

75: Rubinstein, M. amd Obukhov, S. P., Power-Law-Like Stress Relaxation of Block Copolymers: Disentanglement Regimes, *Macromolecules* ***1993***, 26, 1740-1750

76: Rubinstein, M.; Panyukov, S., Nonaffine Deformation and Elasticity of Polymer Networks, *Macromolecules* ***1997***, 30, 8036-8044

77: Heinrich, G.; Straube, E., On The Strength And Deformation Dependence Of The Tube-Like Topological Constraints Of Polymer Networks, Melts And Concentrated-Solutions .2. Polymer Melts And Concentrated-Solutions, *Acta Polymerica* ***1984***, 35, 115-119

78: Heinrich, G.; Straube, E., A Theory Of Topological Constraints In Polymer Networks, *Polymer Bulletin* ***1987***, 17, 247-253

79: Roland, C.M.; Mott, P.H., Comment on "Nonaffine Deformation and Elasticity of Polymer Networks", *Macromolecules* ***1998***, 31, 4033-4034

80: Ball, R. C.; Doi, M.; Edwards, S. F.; Warner M., Elasticity of Entangled Networks, *Polymer* ***1981***, 22, 1010-1018

81: Edwards, S. F.; Vilgis, T. A., The effect of entanglements in rubber elasticity, *Polymer* ***1986***, 27, 483-492

82: Edwards, S. F.; Vilgis, T. A., The tube model theory of rubber elasticity, *Reports on Progress in Physics* ***1988***, 51, 243-297

83: Dossin, L. M.; Graessley, W. W., Rubber Elasticity of Well-Characterized Polybutadiene Networks, *Macromolecules* ***1979***, 12, 123-130

84: Xu, P.; Mark, J. E., Biaxial Extension Studies Using Inflation Of Sheets Of Unimodal Model Networks, *Rubber Chemistry And Technology* ***1990***, 63, 276-284

85: Bhawe, D. M.; Cohen, C.; Escobedo, F. A., Formation and Characterization of Semiflexible Polymer Networks via Monte Carlo Simulations, *Macromolecules* ***2004***, 37, 3924-3933

86: Bhawe, D. M.; Cohen, C.; Escobedo, F. A., Stepwise Elastic Bahavior in a Model Elastomer, *Physical Review Letters* ***2004***, 93, 257804

87: Bhawe, D. M.; Cohen, C.; Escobedo, F. A., Effect of chain stiffness and entanglements on the elastic behavior of end-linked elastomers, *The Journal of Chemical Physics* ***2005***, 123, 014909

88: Carri, G. A.; Batman, R.; Varshney, V.; Dirama, T. E., A Monte Carlo simulation study of the mechanical and conformational properties of networks of helical polymers. I. General concepts, *Polymer* ***2005***, 46, 3809-3817

89: Batman, R.; Carri, G. A., A Monte Carlo simulation study of the mechanical and conformational properties of networks of helical polymers. Part II. The effect of temperature, *Polymer* ***2005***, 46, 10128-10138

90: Duering, E. R.; Kremer, K.; Grest, G. S., Structure and relaxation of end-linked polymer networks, *The Journal of Chemical Physics* ***1994***, 101, 8169-8192

91: Everaers, R.; Kremer, K., Test of the Foundations of Classical Rubber Elasticity, *Macromolecules* ***1995***, 28, 7291-7294

92: Grest, G. S.; Putz, M.; Everaers, R.; Kremer, K, Stress-strain relation of entangled polymer networks, *Journal of Non-Crystalline Solids* ***2000***, 274, 139-146

93: Jianping, G.; Weiner, J. H., Nature of Stress on the Atomic Level in Dense Polymer Systems, *Science* ***1994***, 266, 748-752

94: R. C. Picu and G. Loriot and J. H. Weiner, Toward a unified view of stress in small-molecular and in macromolecular liquids, *The Journal of Chemical Physics* ***1999***, 110, 4678-4686

95: Patel, S. K.; Malone, S.; Cohen, C.; Gillmor, J. R.; Colby, R. H., Elastic-Modulus And Equilibrium Swelling Of Poly(Dimethylsiloxane) Networks, *Macromolecules* ***1992***, 25, 5241-5251

96: Queslel, J. P.; Mark, J. E., Molecular Interpretation Of The Moduli Of Elastomeric Polymer Networks Of Known Structure, *Advances In Polymer Science* ***1984***, 65, 135-176

97: Kroger, M. and Hess, S., Rheological evidence for a dynamical crossover in polymer melts via nonequi, *Physical Review Letters* ***2000***, 85, 1128-1131

98: Masubuchi, Y.; Takimoto, J. I.; Koyama, K.; Ianniruberto, G.; Marrucci, G.; Greco, F., Brownian simulations of a network of reptating primitive chains, *Journal Of Chemical Physics* ***2001***, 115, 4387-4394

99: Masubuchi, Y.; Watanabe, H.; Ianniruberto, G.; Greco, F.; Marrucci, G., Primitive chain network simulations on dielectric relaxation of linear polymers under shear flow, *Nihon Reoroji Gakkaishi* ***2004***, 32, 197-202

100: Masubuchi, Y.; Ianniruberto, G.; Greco, F.; Marrucci, G., Molecular simulations of the long-time behaviour of entangled polymeric liquids by the primitive

chain network model, *Modelling And Simulation In Materials Science And Engineering* ***2004***, 12, S91-S100

101: Masubuchi, Y.; Ianniruberto, G.; Greco, F., Biased hooking for primitive chain network simulations of block copolymers, *Korea-Australia Rheology Journal* ***2006***, 18, 99-102

102: Masubuchi, Y.; Ianniruberto, G.; Greco, F.; Marrucci, G., Primitive chain network model for block copolymers, *Journal Of Non-Crystalline Solids* ***2006***, 352, 5001-5007

103: Masubuchi, Y.; Ianniruberto, G.; Greco, F.; Marrucci, G., Primitive chain network simulations for branched polymers, *Rheologica Acta* ***2006***, 46, 297-303

104: Furuichi, K.; Nonomura, C.; Masubuchi, Y.; Ianniruberto, G.; Greco, F.; Marrucci, G., Primitive chain network simulations of damping functions for shear, uniaxial, biaxial and planar deformations, *Nihon Reoroji Gakkaishi* ***2007***, 35, 73-77

105: Furuichi, K.; Nonomura, C.; Masubuchi, Y.; Watanabe, H.; Ianniruberto, G.; Greco, F.; Marrucci, G., Entangled polymer orientation and stretch under large step shear deformations in primitive chain network simulations, *Rheologica Acta* ***2008***, 47, 591-599

106: Yaoita, T. and Isaki, T. and Masubuchi, Y. and Watanabe, H. and Ianniruberto, G. and Greco, F. and Marrucci, G., Highly entangled polymer primitive chain network simulations based on dynamic tube dilation, *Journal Of Chemical Physics* ***2004***, 121, 12650-12654

108: Yaoita, T.; Isaki, T.; Masubuchi, Y.; Watanabe, H.; Ianniruberto, G.; Greco, F.; Marrucci, G., Statics, linear, and nonlinear dynamics of entangled polystyrene melts simulated through the primitive chain network model, *Journal Of Chemical Physics* ***2008***, 128,

110: de Gennes, P. G., Reptation of a Polymer Chain in the Presence of Fixed Obstacles, *The Journal of Chemical Physics* ***1971***, 55, 572-579

111: de Gennes, P. G., ***Scaling Concepts in Polymer Physics***, 1979

112: Doi, M.; Edwards, S. F., ***The Theory of Polymer Dynamics***, 1986

113: Doi, M., Explanation For The 3.4 Power Law Of Viscosity Of Polymeric Liquids On The Basis Of The Tube Model, *Journal Of Polymer Science Part C-Polymer Letters* ***1981***, 19, 265-273

114: Milner, S. T., Reptation and Contour-Length Fluctuations in Melts of Linear Polymers, *Physical Review Letters* , 81, 725

115: Graessley, W. W., Entangled Linear, Branched And Network Polymer Systems - Molecular Theories, *Advances In Polymer Science* ***1982***, 47, 67-117

116: Watanabe, H., Viscoelasticity and dynamics of entangled polymers, *Progress in Polymer Science* ***1999***, 24, 1253-1403

117: Marrucci, G., Dynamics of entanglements: A nonlinear model consistent with the Cox-Merz rule, *Journal of Non-Newtonian Fluid Mechanics* ***1996***, 62, 279-289

118: Ianniruberto, G.; Marrucci, G., On compatibility of the Cox-Merz rule with the model of Doi and Edwards, *Journal of Non-Newtonian Fluid Mechanics* ***1996***, 65, 241-246

119: Mead, D. W.; Larson, R. G.; Doi, M., A molecular theory for fast flows of entangled polymers, *Macromolecules* ***1998***, 31, 7895-7914

120: Milner, S. T.; McLeish, T. C. B.; Likhtman, A. E., Microscopic theory of convective constraint release, *Journal of Rheology* ***2001***, 45, 539-563

121: Khaliullin, R. N.; Schieber, J. D., Analytic Expressions for the Statistics of the Primitive-Path Length in Ent, *Physical Review Letters* ***2008***, 100, 188302-4

122: Larson, R.G, Looking inside the entanglement "Tube" using molecular dynamics Simulations, *Journal of Polymer Science Part B-Polymer Physics* ***2007***, 45, 3240-3248

123: Larson, R. G.; Zhou, Q.; Shanbhag, S.; Park, S. J., Advances in Modeling of Polymer Melt Rheology, *American Institute of Chemical Engineering* ***2007***, 53, 542-548

124: Hoy, R. S.; Grest, G. S., Entanglements of an end-grafted polymer brush in a polymeric matrix, *Macromolecules* ***2007***, 40, 8389-8395

125: McCarthy, D. W.; Mark, J. E.; Clarson, S. J.; Schaefer, D. W., Synthesis, structure, and properties of hybrid organic-inorganic composites based on polysiloxanes. II. Comparisons between poly(methylphenylsiloxane) and poly(dimethylsiloxane), and between titania and silica, *Journal Of Polymer Science Part B-Polymer Physics* ***1998***, 36, 1191-1200

126: McCarthy, D. W.; Mark, J. E.; Schaefer, D. W., Synthesis, structure, and properties of hybrid organic-inorganic composites based on polysiloxanes. I. Poly(dimethylsiloxane) elastomers containing silica, *Journal Of Polymer Science Part B-Polymer Physics* ***1998***, 36, 1167-1189

127: Vieweg, S.; Unger, R.; Heinrich, G.; Donth, E., Comparison of dynamic shear properties of styrene-butadiene vulcanizates filled with carbon black or polymeric fillers, *Journal of Applied Polymer Science* ***1999***, 73, 495-503

128: Payne, A. R., Hysteresis of rubbers loaded with carbon black, *Nature* ***1964***, 201, 1213

129: Harwood, J. A. C.; Mullins, L.; Payne, A. R., Tensile stress softening effects in pure gum and filler loaded vulcanizates, *Journal of Polymer Science Part B-Polymer Letters* ***1965***, 3, 119

130: Harwood, J. A. C.; Mullins, L.; Payne, A. R., Stress softening in natural rubber vulcanizates .2. stress softening effects in pure gum and filler loaded rubbers, *Journal of Applied Polymer Science* ***1965***, 9, 3011

131: Lacevic, N.; Gee R. H.; Saab, A.; Maxwell R., Computational exploration of polymer nanocompsite mechanical property modification via cross-linking topology, *The Journal of Chemical Physics* ***2008***, 129, 124903

132: Ash, B. J.; Schadler, L. S.; Siegel, R. W., Glass transition behavior of alumina/ polymethylmethacrylate nanocomposites, *Materials Letters* ***2002***, 55, 83-87

133: Zheng, L.; Farris, R. J.; Coughlin, E. B., Novel polyolefin nanocomposites: Synthesis and characterizations of metallocene-catalyzed polyolefin polyhedral oligomeric silsesquioxane copolymers, *Macromolecules* ***2001***, 34, 8034-8039

134: Huber, G.; Vilgis, T. A., On the mechanism of hydrodynamic reinforcement in elastic composites, *Macromolecules* ***2002***, 35, 9204-9210

135: Hooper, J. B.; Schweizer, K. S., Theory of phase separation in polymer nanocomposites, *Macromolecules* ***2006***, 39, 5133-5142

136: Hooper, J. B.; Schweizer, K. S., Real space structure and scattering patterns of model polymer nanocomposites, *Macromolecules* ***2007***, 40, 6998-7008

137: Striolo, A; McCabe, C.; Cummings, P. T., Effective interactions between polyhedral oligomeric sislesquioxanes dissolved in normal hexadecane from molecular simulation, *Macromolecules* ***2005***, 38, 8950-8959

138: Striolo, A.; McCabe, C.; Cummings, P. T., Organic-inorganic telechelic molecules: Solution properties from simulations, *Journal of Chemical Physics* ***2006***, 125,

139: Striolo, A.; McCabe, C.; Cummings, P. T.; Chan, E. R.; Glotzer, S. C., Aggregation of POSS monomers in liquid hexane: A molecular-simulation study, *Journal of Physical Chemistry B* ***2007***, 111, 12248-12256

140: Chan, E. R.; Striolo, A.; McCabe, C.; Cummings, P. T.; Glotzer, S. C., Coarse-grained force field for simulating polymer-tethered silsesquioxane self-assembly in solution, *Journal of Chemical Physics* ***2007***, 127,

141: Shanbhag, S.; Larson, R. G.; Takimoto, J.; Doi, M., Deviations from Dynamic Dilution in the Terminal Relaxation of Star Polymers*, Physical Review Letters* ***2001****, 87, 195502*